Geothermics 136 (2026) 103596

Contents lists available at ScienceDirect

Geothermics

journal homepage: www.elsevier.com/locate/geothermics

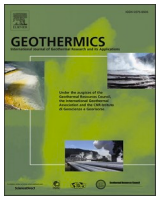

Fracture properties, structural heterogeneity, and permeability in the Þeistareykir geothermal system, NE Iceland

Aastha [a,*], Emma Bramham [a], Andy Nowacki [a], Nick Shaw [a], Anette Mortensen [b], David Healy [a]

[a] Geosolutions Leeds, School of Earth, Environment & Sustainability, University of Leeds, Leeds, United Kingdom
[b] Landsvirkjun, Reykjavik, Iceland

ARTICLE INFO

Keywords:
Natural fractures
Acoustic image logs
Core
Fluid flow
Þeistareykir geothermal system
Iceland

ABSTRACT

Permeability in the Þeistareykir geothermal system of Iceland is structurally controlled. Natural fracture networks are abundant in Þeistareykir and contribute significantly to fluid flow. Understanding which features enhance permeability and hydraulic conductivity, and how their properties interact with lithology and reservoir structure, is key to predicting reservoir behaviour. To address this, we utilise a range of borehole data to characterise natural fractures in terms of their occurrence, orientation, relative distribution, their relationship with the major lithological units and permeable flow zones in the subsurface. Results show systematic variations in fracture density, thickness, and distribution pattern across different lithologies and depths, with orientations ranging from NNW-SSE, N-S, NNE-SSW to NE-SW. Fractures exhibit the highest intensity in the deeper acidic intrusive units or coarser grained basalt with a predominant N-S-trend and bimodal dip distribution. However, permeability is controlled by a complex interplay of fracture geometry, openness and connectivity rather than simply high fracture abundance or a preferential set of fractures. Permeable feed zones show diverse structural expressions, ranging from high-density fracture clusters and large-aperture fractures to intensely fractured damage zones and multiple intersecting fracture sets. These findings demonstrate that the structural character of the potential fluid-flow channels is highly variable in Þeistareykir. The results of this study can be incorporated into fracture and flow models to enhance our understanding of the permeability distribution and fluid pathways in the Þeistareykir geothermal system.

1. Introduction

Structures such as fractures and faults play an important role in heat extraction from geothermal reservoirs located in active tectonic regions, as they regulate geothermal fluid movement in the subsurface (Rowland and Sibson, 2004). Depending on their characteristics, fracture networks can act as either pathways or barriers to fluid flow and can directly impact permeability distribution and reservoir productivity (e.g., Chen et al., 2021; Narr et al., 2006; Pérez-Flores et al., 2017). Other factors being equal, interconnected, permeable structural networks can provide sustainable routes for geothermal fluid extraction and recharge (Bense et al., 2013; Brogi, 2008; Caine et al., 1996; Faulds and Hinz, 2015; Rowland and Sibson, 2004; Sibson, 1996). A proper understanding of the distribution, structural complexity, and physical and hydraulic properties of fractures is therefore often essential for sustainable use of the resource.

High-temperature geothermal systems with temperatures exceeding 200 °C are found on the active plate boundaries of the Northern Volcanic Zone (NVZ), which represents the surface extension of the Mid-Atlantic Ridge in the northern part of Iceland (Arnórsson, 1995). The NVZ is characterized by extensional structures, eruptive fissures and transform faults, creating seven volcanic systems and their fissure swarms (Einarsson, 2008; Hjartardóttir et al., 2016; Pedersen et al., 2009). This study focusses on the Þeistareykir fissure swarm of the NVZ in NE Iceland. The Þeistareykir geothermal system spans approximately 25–30 km^2 on the surface (Ármannsson, 2016) and is characterised by extensive fracturing throughout the area. Many wells have been drilled in this field, and despite the small field size, the temperature and permeability distribution are found to be highly variable in the geothermal system (Guðmundsdóttir et al., 2018). Temperature reversal is observed in some wells drilled within the main fault and fissure system (Jóhannsson, 2011; Kajugus, 2012). It is critical to understand the mechanism

* Corresponding author.
E-mail address: aastha1@leeds.ac.uk (Aastha).

https://doi.org/10.1016/j.geothermics.2026.103596
Received 8 October 2025; Received in revised form 15 December 2025; Accepted 2 January 2026

constraining heat and fluid flow in this structurally-controlled geothermal system.

This paper presents the results of a fracture characterisation study in Þeistareykir, through a close integration of geological, geophysical, petrophysical, and dynamic data from six production wells and a cored shallow exploration well in the Þeistareykir geothermal field. Cores, and acoustic image logs are analysed to document natural fracture characteristics, including the types of natural fractures occurring in the reservoir, their distribution, orientation, density and thickness. Drill cuttings and geophysical logging data aid in the interpretation of the major lithological units. This leads to an understanding of the regional fracture patterns, their spatial and vertical heterogeneity and the variations in fracture characteristics in different geologic units. This is then correlated with the permeable feed zones identified in the wells based on temperature logs, circulation losses and spinner logging. We establish the structural character of these permeable feed zones, which represent the subsurface fluid flow channels in the reservoir.

2. Geological and structural context

The Þeistareykir fissure swarm is N–S-trending, 7–8 km wide and 70–80 km long, located within the N–S-oriented Northern Volcanic Zone (NVZ), and intersected by the WNW-ESE oriented Tjörnes Fracture Zone (TFZ) (Figure 1; Khodayar et al., 2018; Sæmundsson, 2007, 1974; Sveinbjornsdóttir et al., 2013). Þeistareykir is the westernmost of the seven volcanic systems in the NVZ. The area is characterized by large normal faults along its western rim, with displacements of up to 200–300 m in the Lambafjöll and Tjörnes mountains, along with numerous rift fissures (Magnúsdóttir and Brandsdóttir, 2011). Although the volcanic system exhibits features of a central volcano, a true caldera structure has not formed (Einarsson, 2008). The central volcanic formations are dominated by Holocene lava fields, while the surrounding mountains are older, with the southern Tjörnes mountains being less than 900,000 years old (Camps et al., 2011; Magnúsdóttir and Brandsdóttir, 2011). Lava flows, mainly shield lavas, cover the surface, dating from shortly before and after the termination of the last glaciation period (Óskarsson, 2016). Notable lava formations include Stóravítishraun (11–12,000 yr), Skildingahraun (>14,500 yr), Borgarhraun (8–10,000 yr), and the most recent Þeistareykjahraun lava (2400 yr) (Gíslason et al., 1984; Sæmundsson et al., 2012).

The Þeistareykir geothermal field at the intersection of the NVZ and TFZ is subject to the tectonics of both rift and transform plate boundaries, leading to a highly fractured-reservoir (Liotta et al., 2021; Pasquarè Mariotto et al., 2015). Previous surface structural studies are reported in the area, mainly based on aerial photographs and satellite images, to understand the overall tectonic configuration of the Þeistareykir field. Part of the Þeistareykir fissure swarm was mapped by Magnúsdóttir and Brandsdóttir (2011) while Hjartardóttir (2013) provides an in-depth study of the orientations and characteristics of fractures and eruptive fissures in the Northern Volcanic Rift Zone (NVZ). The area is characterised by normal faults, extension fractures and eruptive fissures with an overall N-, NE- and NNE-strike, however, changes in fracture orientations are more prominent in the central and northern part of the fissure swarm, where it connects with the Húsavík-Flatley Fault (Hjartardóttir, 2013). Bonali et al. (2019) studied in detail the rift-transform development in the northern part of the fissure

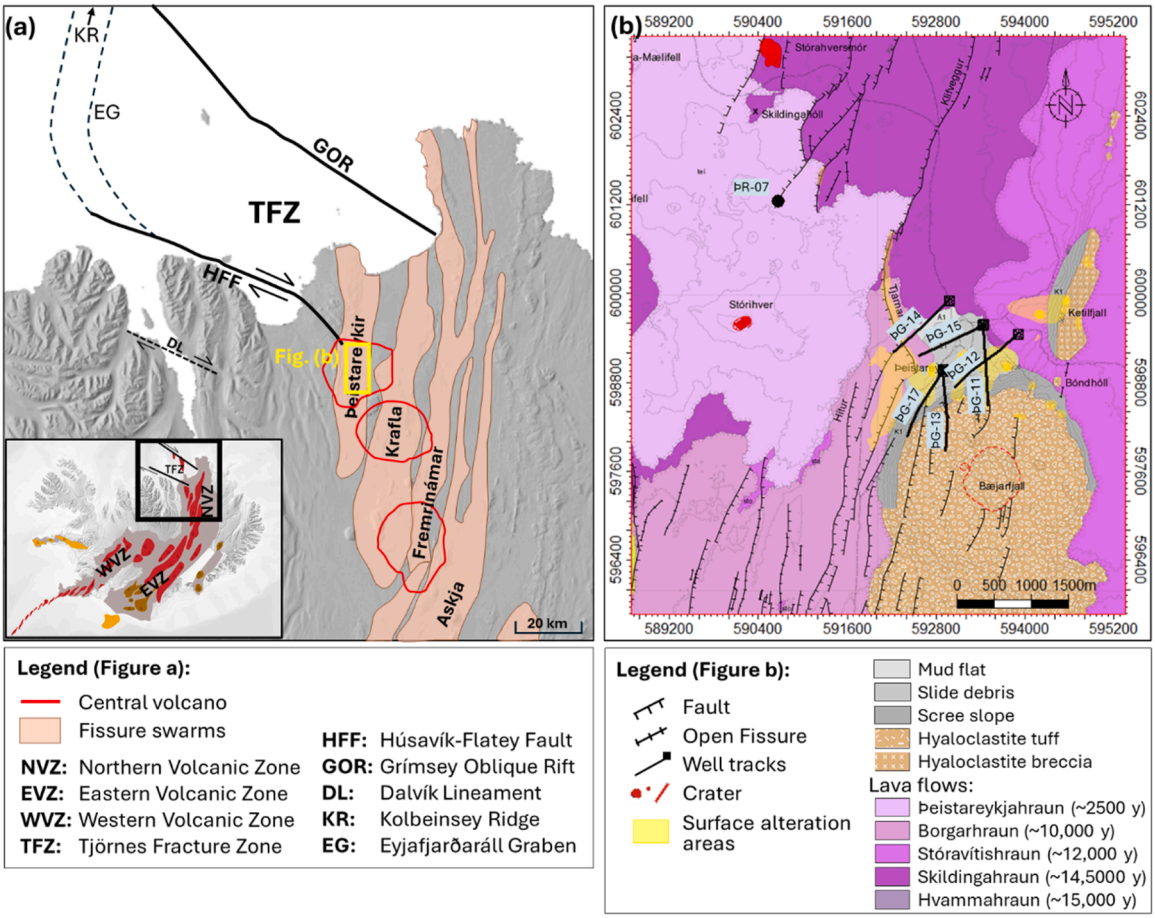

Fig. 1. (a) A simplified map of northern Iceland showing the major tectonic structures of the Northern Volcanic Zone and Tjörnes Fracture Zone. Outlines of the volcanic centres and fissure swarms of NVZ are from Hjartardóttir (2013). (b) Geological map of the Þeistareykir geothermal area (from Sæmundsson et al., 2012) showing locations of the studied wells.

swarm. 1537 post-Late Glacial Maximum structures were mapped in an area of 85 km^2 between the Húsavík-Flatley Fault (HFF) and Grimsey Volcanic Zone (GVZ). The variations in the fracture patterns are suggested to be a combination of the possible interaction with transform faults of the TFZ that create local diversions in the regional fracture trend and the presence of substrate faults that may have guided later fracture propagation upwards (Bonali et al., 2019; Tibaldi et al., 2016) .

The Þeistareykir high-temperature geothermal area in the eastern part of the fissure swarm spans approximately 25–30 km^2, primarily in the area northwest and north of Mt. Bæjarfjall (Fig. 1). It is subdivided into five N–S-oriented sub-areas, each with varying reservoir temperatures estimated by gas geochemistry of fumaroles (Ármannsson, 2016; Saby et al., 2020). A notable low-resistivity anomaly spanning the centre of the system encompasses surface geothermal activity and is indicative of the geothermal heat source (Karlsdóttir et al., 2012; Magnúsdóttir and Brandsdóttir, 2011). Geothermal drilling operations began in 2002, resulting in the development of the geothermal field with 20 wells ranging in depth from 1723 m to 2799 m and reaching temperatures of 347 °C. Exploitation commenced in 2017, with the installation of two generating units producing 45 MWe, making Þeistareykir the fourth-largest geothermal station in Iceland.

3. Data and methods

3.1. Drilling and geophysical logging data

This study incorporates drilling and wireline logging data from six production wells in the Þeistareykir geothermal field, namely ÞG-11, ÞG-12, ÞG-13, ÞG-14, ÞG-15 and ÞG-17 (Fig. 1b). A conventional basic suite of well-logs is available in all of these wells, including XY caliper log, gamma ray, resistivity (16″ and 64″) and neutron-neutron, along with the description and interpretation of lithology, alteration, intrusions and circulation losses. Indications of feed zones are provided based on temperature logging, losses in circulation and flow measurements with spinner (Guðmundsdóttir et al., 2018).

3.2. Acoustic borehole televiewer (BHTV) imaging

The six wells were imaged by acoustic borehole televiewer using the ABI-43 (Acoustic Borehole Imaging, 43 mm diameter) logging probe, deployed by ÍSOR (Fig. 1, Table 1). Acoustic borehole televiewer (BHTV) logging generates images of the inside of a borehole by using ultrasonic pulses. These logs provide detailed, 360° unwrapped oriented images of borehole walls over sections extending up to several kilometres (Poppelreiter et al., 2010; Zemanek et al., 1970). The BHTV tool emits and receives ultrasonic signals that reflect off the borehole walls, capturing two types of information: the travel time of the sonic wave, which depends on the borehole's shape and diameter, and the returning amplitude of the sonic wave, which relates to the acoustic impedance of the borehole wall (Hurley, 2004). Both of these parameters, the ultrasonic travel time and acoustic amplitude are recorded and processed into image logs along the borehole. These logs can therefore detect fractures with sufficient acoustic impedance contrast and provide details on their orientation and apparent thickness. Planar features intersecting the borehole appear as sinusoids on these image logs (Hurley, 2004; Kraal et al., 2021; Lai et al., 2018).

Image interpretation is performed using Techlog wellbore software platform with approximately 9900 m of BHTV images analysed for fracture picking. The fractures are classified based on a combination of different image characteristics, including acoustic amplitude (high and low amplitude), visibility of the fracture trace in the travel time image and confidence on feature picking (high/medium/low). The level of confidence in fracture interpretation is dependent on a number of factors such as borehole conditions and image quality, continuity of the fracture trace across the borehole diameter and their visualisation as sharp planar features or vague and uneven traces (Dezayes et al., 2005; Massiot et al., 2015; Zahmatkesh et al., 2016). This kind of fracture identification and distinct categorisations helps with a detailed structural characterisation at the borehole scale. For example, a high acoustic amplitude response can occur due to mineral infillings of calcite, quartz or indurated clay, suggesting the presence of closed fractures or mineralized vein fills (Davatzes and Hickman, 2010; Milloy et al., 2015). On the other hand, low amplitude features with good visibility in the travel time image and a high level of confidence may represent possibly open fractures. However, it cannot be determined on the basis of image logs alone, whether such fractures enhance permeability and are open to fluid flow or are partially or completely filled with minerals such as clay, iron oxides or pyrite (Milloy et al., 2015). Therefore, fracture analysis results must be studied in combination with drilling and completion testing data to assess the structural controls on fluid flow in the system.

From the interpreted fracture dataset, structural features are also identified based on their distinct structural characteristics in the image log. For example, indications of possible faults are provided by abrupt termination or truncation of features against a surface or the juxtaposition of different lithologies (Brandão et al., 2024; Hosseini et al., 2015; Massiot et al., 2015; Wennberg et al., 2023). Boundaries between different lithological units are also identified based on a change in the overall acoustic amplitude character (Davatzes and Hickman, 2010). Moreover, fracture density is calculated as the number of fractures per metre depth, with Terzaghi correction applied to remove borehole sampling bias (Terzaghi, 1965). Apparent fracture thickness is estimated directly from the unwrapped acoustic image as the width of the feature exposed on the borehole wall. It is first corrected for fracture dip (Mutonga and Fujimitsu, 2024), and then for borehole deviation to obtain “true fracture thickness” (supplementary Figure A.1). All references to fracture thickness in the result and discussion sections correspond to this true fracture thickness as defined above.

3.3. Core analysis

Cores are extensively used for geological, geochemical, petrophysical and structural studies of subsurface rocks (Tavakoli, 2018). Fracture logging of core and the interpretation of naturally occurring and induced fractures provide important information for the characterization of naturally fractured reservoirs (Kulander et al., 1990). Well ÞR-07 is a shallow exploration well located 1.5 km away from the main production

Table 1
Depth intervals of the Acoustic Borehole Image (ABI) logs in 6 wells used in this study. TD is Total Depth reached by the well.

Well	Date Logged	Bit Size (inch)	Well Deviation at TD (deg)	Well Azimuth at TD (deg)	Depth Interval (m)		Total Length (m)
					Top	Bottom	
ÞG-11	13-Jul-2016	8.5	40	182	764	1401	637
	22-Jul-2016	8.5			1350	2208	858
ÞG-12	27-Sep-2016	8.5	38	220	800	2679	1879
ÞG-13	19-Nov-2016	8.5	32	190	770	2490	1720
ÞG-14	18–19 Jan 2017	8.5	36	227	904	2500	1596
ÞG-15	13-Mar-2017	8.5	34	246	919	2223	1304
ÞG-17	14-Jun-2017	12	39	198	304	720	416
	30-Jun-2017	8.5			950	2494	1544

area in Þeistareykir (Fig. 1). Core samples in this drillhole are available from a depth of 150 m to 458.1 m. Each section of core is examined visually to record the rock type, degree of hydrothermal alteration, fracture occurrence and characteristics. Core photographs and sketches are prepared to complement the descriptive logging, and the data is compiled into structured logs, noting vertical variations along the core length to provide a comprehensive understanding of lithological characteristics and fracture network development.

4. Results and interpretation

4.1. Fracture characteristics in core

We carried out detailed structural logging in the 300 m of core samples available in well ÞR-07 (Fig. 2). The cores exhibit mainly three types of volcanic facies including basalt, volcanic breccia and tuff, that are interbedded with each other and altered with varying intensities depending on the degree of oxidisation, textural or colour changes in the groundmass (Lacasse et al., 2007). Individual fractures are logged through the entire length of core and fracture density is calculated as the number of these fractures per metre length of core. Moreover, intervals of highly fractured rock are observed where individual fractures cannot be segregated, and fractures also occur as clusters in intensely broken or fragmented zones as shown in the core photographs in Fig. 2. Such sections are also highlighted in the fracture density log separately. 161 fractures are logged from a total of 135 m of basaltic units, 21 fractures from 85 m of breccia, 19 fractures from 26 m of tuff and 63 fractures from 59 m of interbedded volcanic breccia and tuff. The highest fracture density is observed in basalt (up to 9 frac/m), whereas broken and fragmented fracture clusters seem to dominate in highly altered breccia units. Hence, we observe that rock characteristics such as lithology and alteration intensity have an impact on fracture distribution and character in different segments of core. The vast majority of fractures seem to be mineralised (secondary mineralisation, mainly quartz or zeolite fillings in amygdules and veins) or the core altered and separated along the fracture plane. Fracture width could be measured only in a few open fractures in basalt and ranges between 0.5–4 mm. Possible slicken-sided surfaces are also observed at some places along fracture planes (Fig. 2).

4.2. Fracture characteristics in image logs

Fractures and other structural features are recognised from BHTV images in the six studied wells, interpreted manually using the dip picking method, and analysed following the methodology described in Section 3.2. Approximately 7000 natural fractures are identified. Some examples of these structural features picked in the borehole images are shown in Fig. 3.

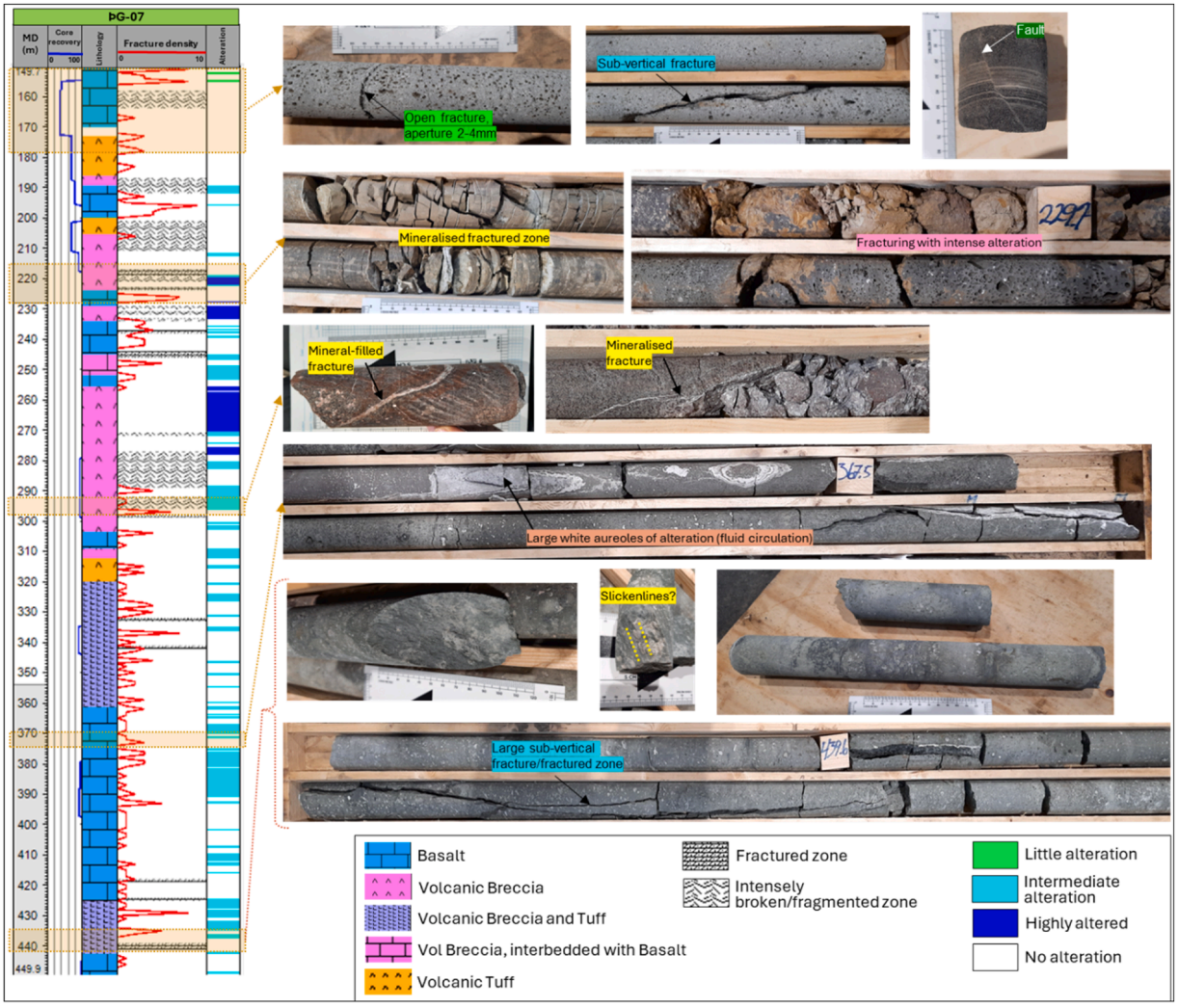

Fig. 2. Core analysis in well ÞR-07 showing the major rock types, degree of fracturing and alteration intensity through the entire length of core (left), along with photographs of structural features observed in the core samples (right). MD is Measured Depth.

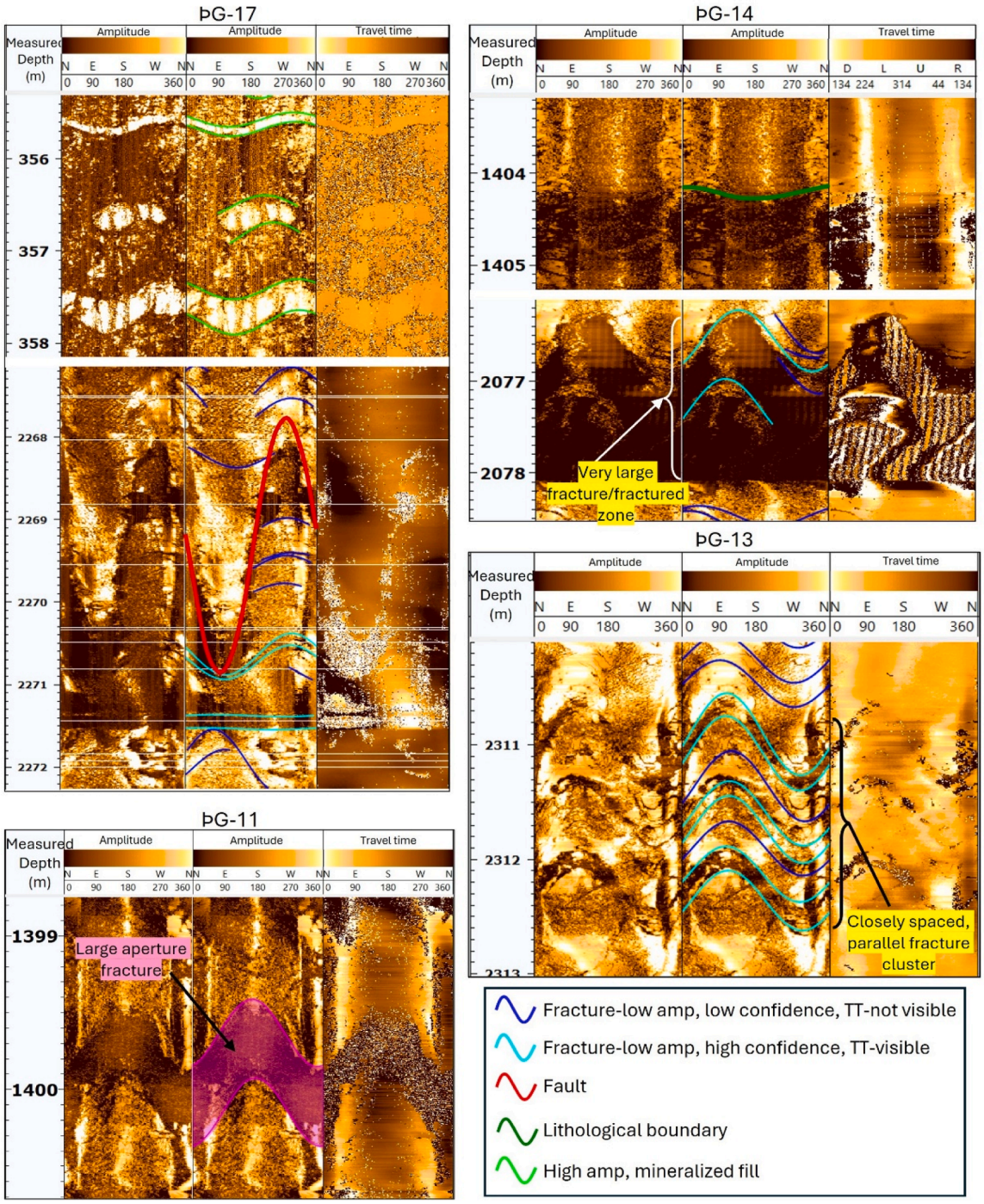

Fig. 3. Examples of interpreted fracture picks and their structural characteristics in the televiewer amplitude and travel time logs from the studied Þeistareykir wells. Fractures are represented as partial or complete sinusoids along the borehole diameter.

4.2.1. Relationship between lithology and fracture character

Cutting samples were collected at every two metres interval in all studied wells during drilling of the production section in the Þeistareykir geothermal field. A detailed description of the different lithologies identified in these cuttings is available, along with the indications of possible intrusions and the main alteration mineralogy (Ásgeirsdóttir et al., 2017a, 2017b, R.St. 2016; Guðjónsdóttir et al., 2017; Poux et al., 2016; Sigurgeirsson et al., 2017). Moreover, the geophysical logs including gamma ray, neutron and resistivity also aid in the interpretation of lithology and geological formations in these volcanic geothermal settings (Steingrímsson, 2011). The major lithological units in Þeistareykir are the hyaloclastites, including basaltic breccia and tuff, which dominates the topmost part of the open-hole section in all wells below the casing shoe. This is followed by multiple layers of basaltic lava flow units, ranging in composition from fine to medium grained basalt and glassy basalt. The acidic intrusive units occur in the deepest part of the wells and are characterised by a high response of gamma ray, neutron and resistivity logs and an intermediate to silicic rock composition. These deeper intrusions range from 300 to 700 m in thickness, although a few 50–60 m thick small intrusions also occur in ÞG-17, ÞG-12 and ÞG-11 (Fig. 4). However, the thick intrusive unit does not occur in ÞG-12 and ÞG-11. Instead, the deepest section in these wells is

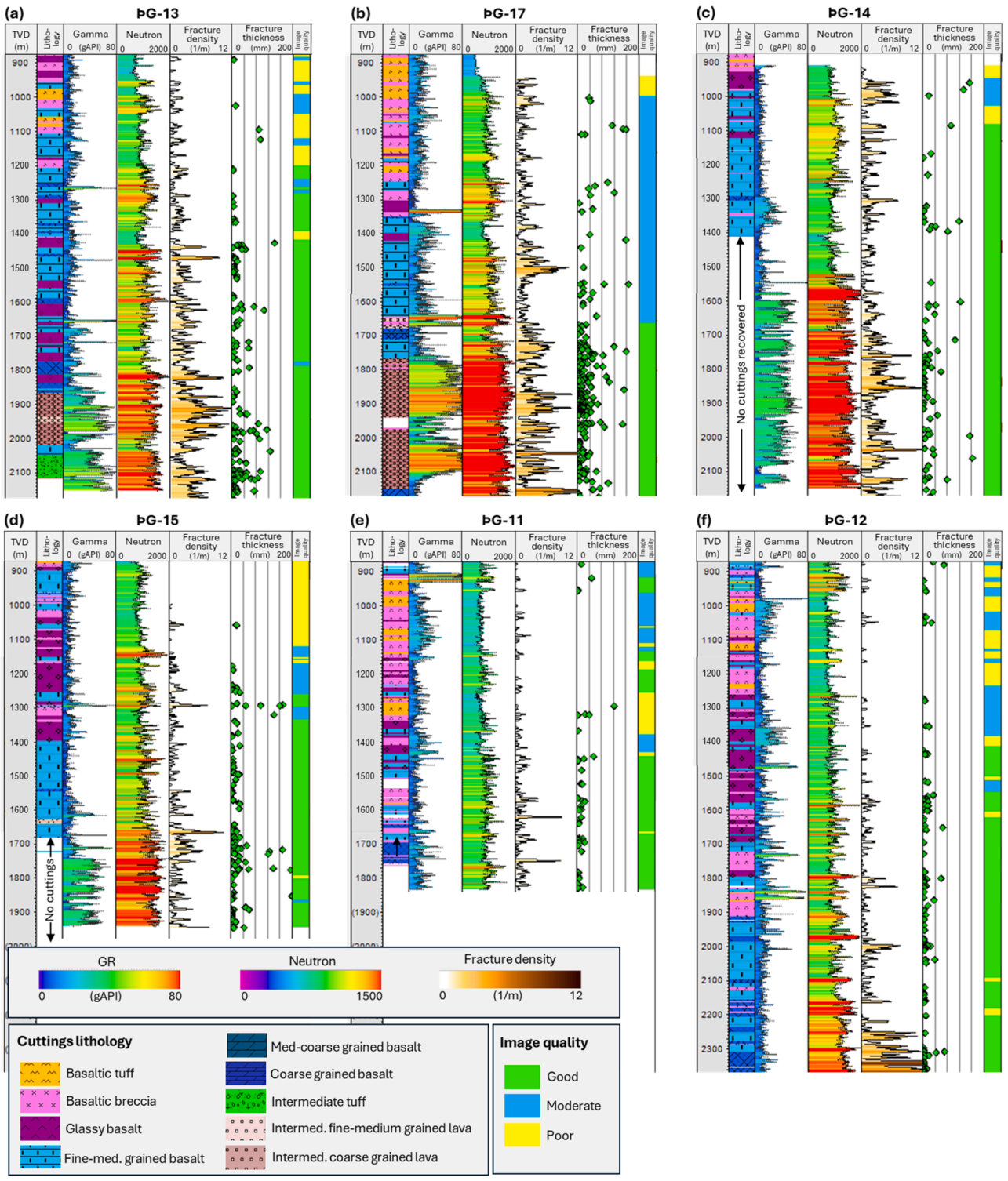

Fig. 4. Plot of wells (a) ÞG-13, (b) ÞG-17, (c) ÞG-14, (d) ÞG-15, (e) ÞG-11, (f) ÞG-12, along True Vertical Depth (TVD) showing cuttings lithology, geophysical logs (gamma ray and neutron), plotted in relation to BHTV-interpreted fracture properties, i.e. fracture density, fracture thicknesses and image log quality.

dominated by a relatively coarser-grained basaltic lava flow.

The fracture properties derived from image analysis are correlated with the major lithological units (Figs. 4 and 5). Fracture density logs highlight the difference in fracture occurrence along wellbores. Fracture density is observed to be the lowest in basaltic breccia and tuff across all the wells. This may be partly due to the poor image quality in hyaloclastites in most wells. It is also clear from the fracture distribution plot in Figs. 5(a) and (b) that the deeper section of the wells, dominated by acidic intrusive units or coarser grained basalts are more densely fractured compared to the shallower lithologies (except for wells ÞG-11 and ÞG-15, where fracture occurrence seems to be uniformly low throughout the borehole). The fractures also exhibit relatively uniform thickness patterns in all wells, with majority of the fractures in the range of 1–50 mm thick (Fig. 5b). However, fracture thickness is more varied in ÞG-17 and this well includes a relatively high number of thicker fractures (>50 mm). There are also two small clusters of large aperture fractures in ÞG-

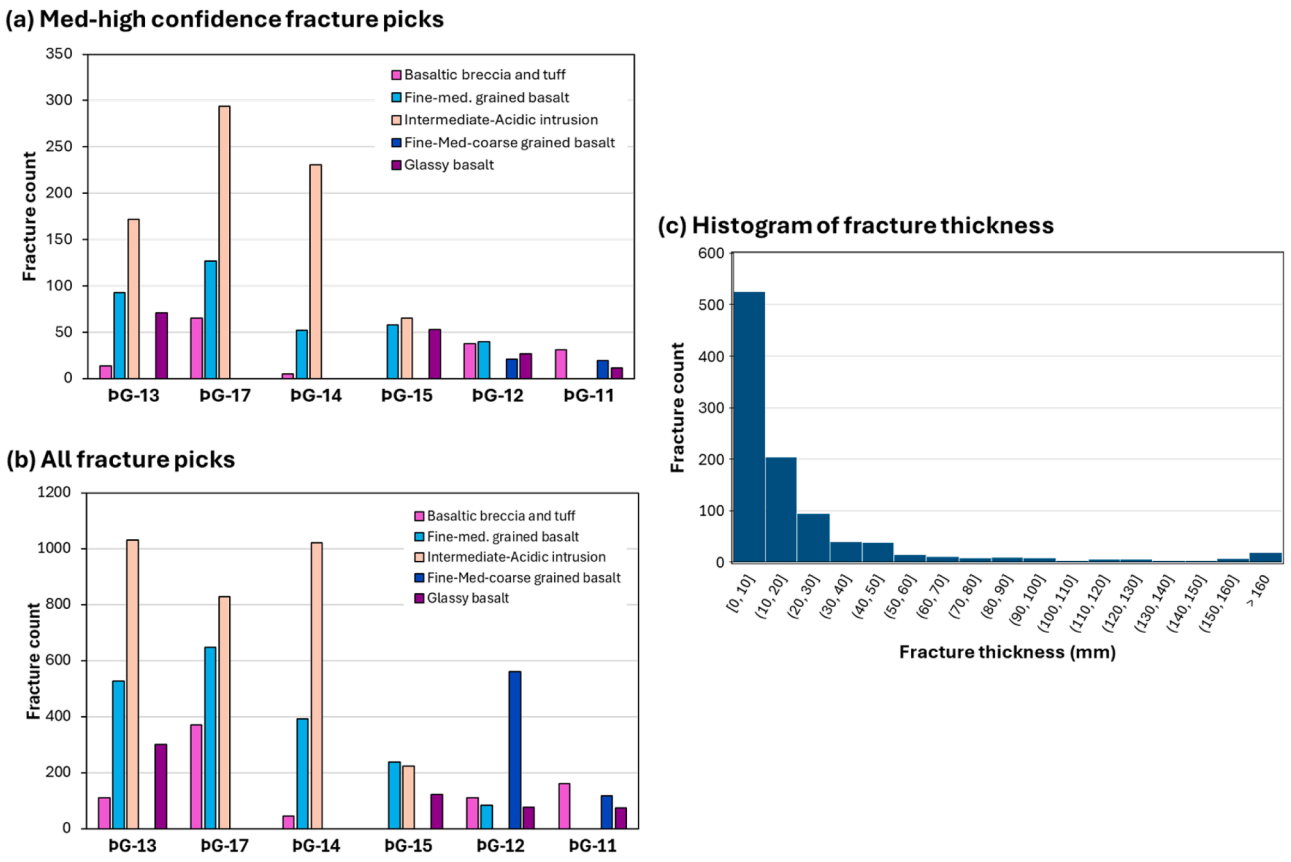

Fig. 5. Plot showing the distribution of fractures in different litho-units across wells, considering (a) medium to high confidence fracture picks, (b) all interpreted fractures. (c) Histogram of all measured fracture thickness in the study area.

15, from 1290–1330 m TVD and 1690–1790 m TVD, where individual fractures reach up to 200 mm in thickness.

4.2.2. *Fracture orientation analysis*

Fig. 6 highlights the relative fracture population in the area and their

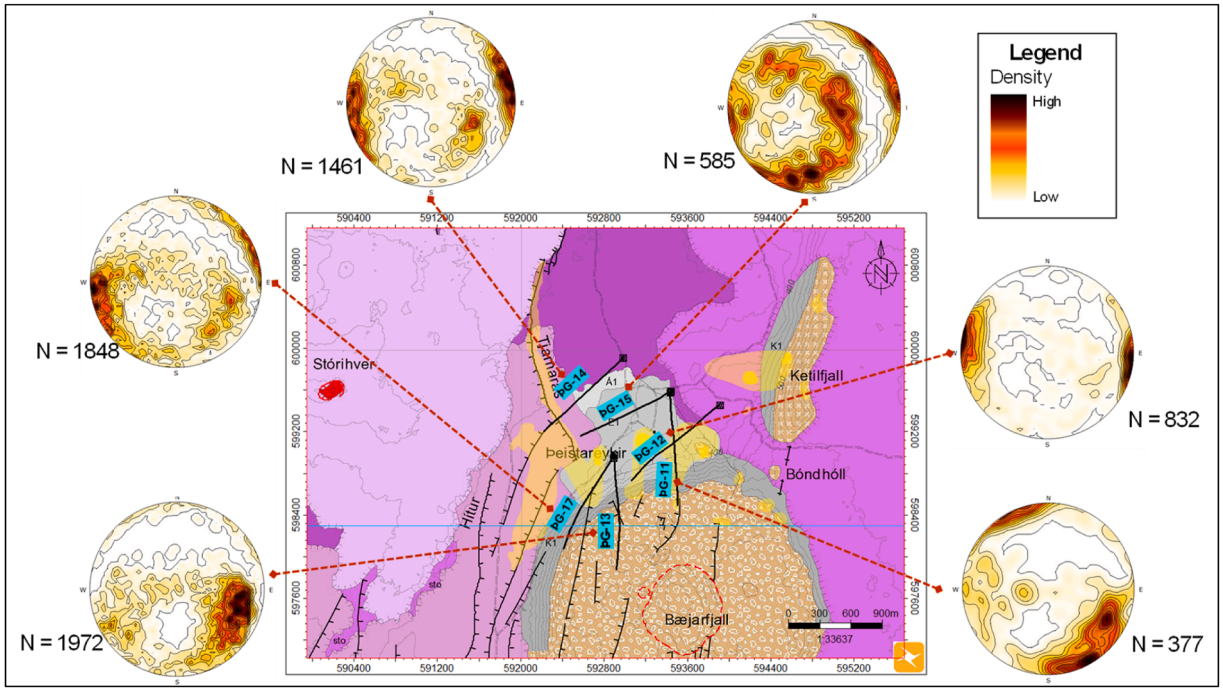

Fig. 6. Geological map of Þeistareykir (zoomed in from Fig. 1b) showing the main production area, with fractures represented as contoured stereo-plots of poles to planes in Schmidt's projection, lower hemisphere for all studied wells. "N" is the total number of fractures interpreted in each well through the entire BHTV-logged interval and the stereonets are also contoured as per this raw fracture count.

orientations measured from the televiewer data indicating overall fracture trends. Fracture occurrence varies spatially, evidenced by the number of fractures interpreted in each well. Wells ÞG-14, ÞG-17 and ÞG-13 located more towards the western part of the field have almost double the number of fracture picks compared to the other wells. Different preferential fracture trends are also observed throughout the field (Fig. 6). Well ÞG-12 has fractures with a well-defined N-S to NNE-SSW strike with high dip angles (>50°), dipping both to the east and west. In wells ÞG-14 and ÞG-17, fracture strikes range from N-S to NNW-SSE. ÞG-14 has both easterly and westerly dip direction, while ÞG-17 is majorly easterly dipping. On the other hand, fractures in well ÞG-15 suggest multiple fracture sets with strikes ranging from E-W, NE-SW, N-S to NNW-SSE and a broad distribution in dip angles from nearly horizontal to vertical. ÞG-13 is majorly westerly dipping with a NNE-SSW orientation and moderate to high dips (>40°). Fractures in ÞG-11 have a NE-SW to ENE-WSW strike with NW-NNW dips (>50 °).

A fracture orientation plot is shown in Fig. 7, including all the high to medium confidence fracture dataset from BHTV interpretation. Fractures are generally steeply dipping and N-S striking across the Þeistareykir wells, but they show clear variations in character both with depth and across different wells. Overall, two principal fracture orientation patterns emerge consistently throughout the field: one set dipping W–NW, and another set displaying more easterly dips. ÞG-13 is consistently dominated by west-dipping fractures. In contrast, ÞG-12, ÞG-14, and ÞG-17 show a bimodal east–west dip distribution pattern throughout their logged intervals. However, the fracture orientation plot of well ÞG-17 reveals more scatter in dip azimuth within basalts and hyaloclastite units. In ÞG-14, the upper part of the well (i.e. fine-medium grained basaltic lava flows) is dominated by very steep, westward-dipping fractures, while at greater depths (i.e. inter-acidic intrusive unit) fracture dips become shallower and rotate toward a near-north orientation. When all the low confidence fracture picks are included in the analysis, the overall dip distribution broadens, with an increase of moderate to low dip angles, secondary dip directions becoming more evident and depth-related fracture trends becoming less distinct. However, the dominance of steep, bimodal E-W fracture pattern remains visible, confirming that they are not artefacts of data uncertainty but reflect distinct structural domains within the field.

4.3. Structural observations in permeable feed zones

Of all the fractures interpreted from BHTV logs, only some play a role in fluid movement in the subsurface. To understand these structurally-driven fluid flow channels, the interpreted fracture datasets are correlated with permeability indications from drilling data, circulation losses, temperature logs and spinner logging carried out after drilling. Fig. 8 provides the depth distribution of permeable feed zones in the studied wells and ranked from small, medium to large based on their relative sizes (Guðmundsdóttir et al., 2018). Figs. 9–14 provide detailed insights into the medium to large feed zones by correlating all geophysical logging data with fracture interpretation from televiewer. By analysing the fracture corridors within these permeable zones, the overall structural character of the potential fluid-flow channels can be inferred, as discussed in the next section.

Well ÞG-14

Four medium to large permeable zones are identified in well ÞG-14 as shown in the composite log section in Fig. 9. Feed zone (ÞG-14-FZ2) at 1422 m is located in the fine-medium grained basaltic lava flow and is the largest in the well, identified by changes in temperature, spinner, circulation losses and large caving in caliper log (Guðjónsdóttir et al., 2017). Another medium-sized feed zone at 1825 m (ÞG-14-FZ3) is located in the intermediate-acidic intrusive unit and evidenced by temperature and spinner logs. The fracture occurrence around 1422 m seems to be low based on the fracture density log in Fig. 9. However, a zoomed in section of the borehole wall from televiewer shows a sharp change in image character from 1438–1441 m and 1444–1445 m.

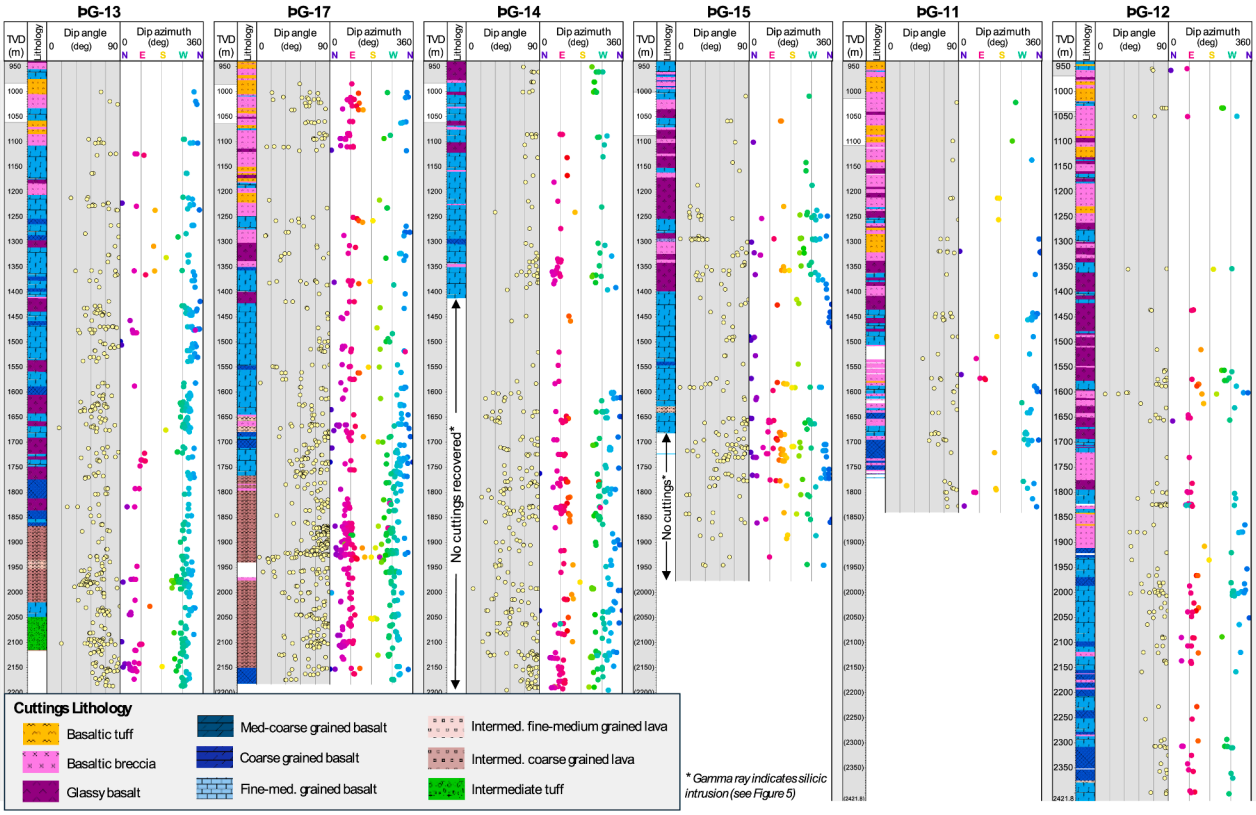

Fig. 7. Dip angle and dip azimuth plots illustrating fracture orientations across all wells, shown with depth and in relation to the major lithological units. Only medium- to high-confidence fracture picks from BHTV interpretation are included. Depth in the left column is the True Vertical Depth (TVD).

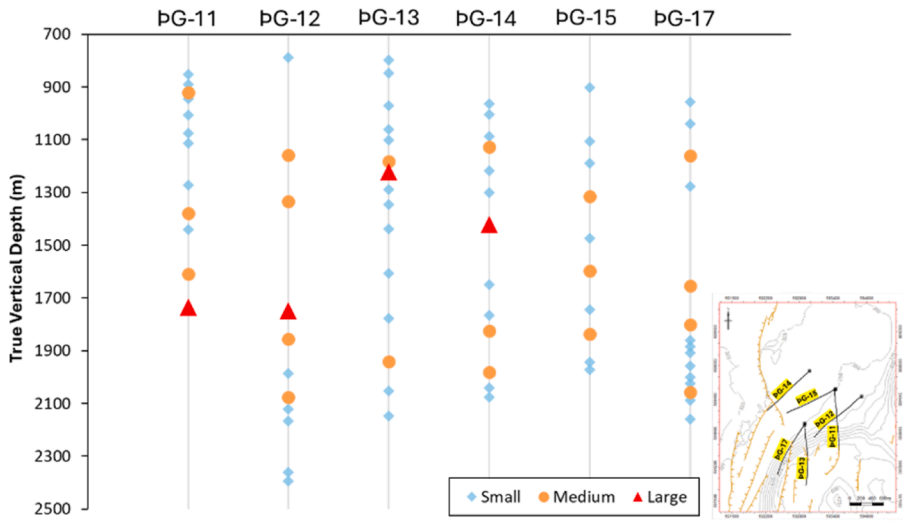

Fig. 8. Vertical feedzone distribution in Þeistareykir in the studied wells.

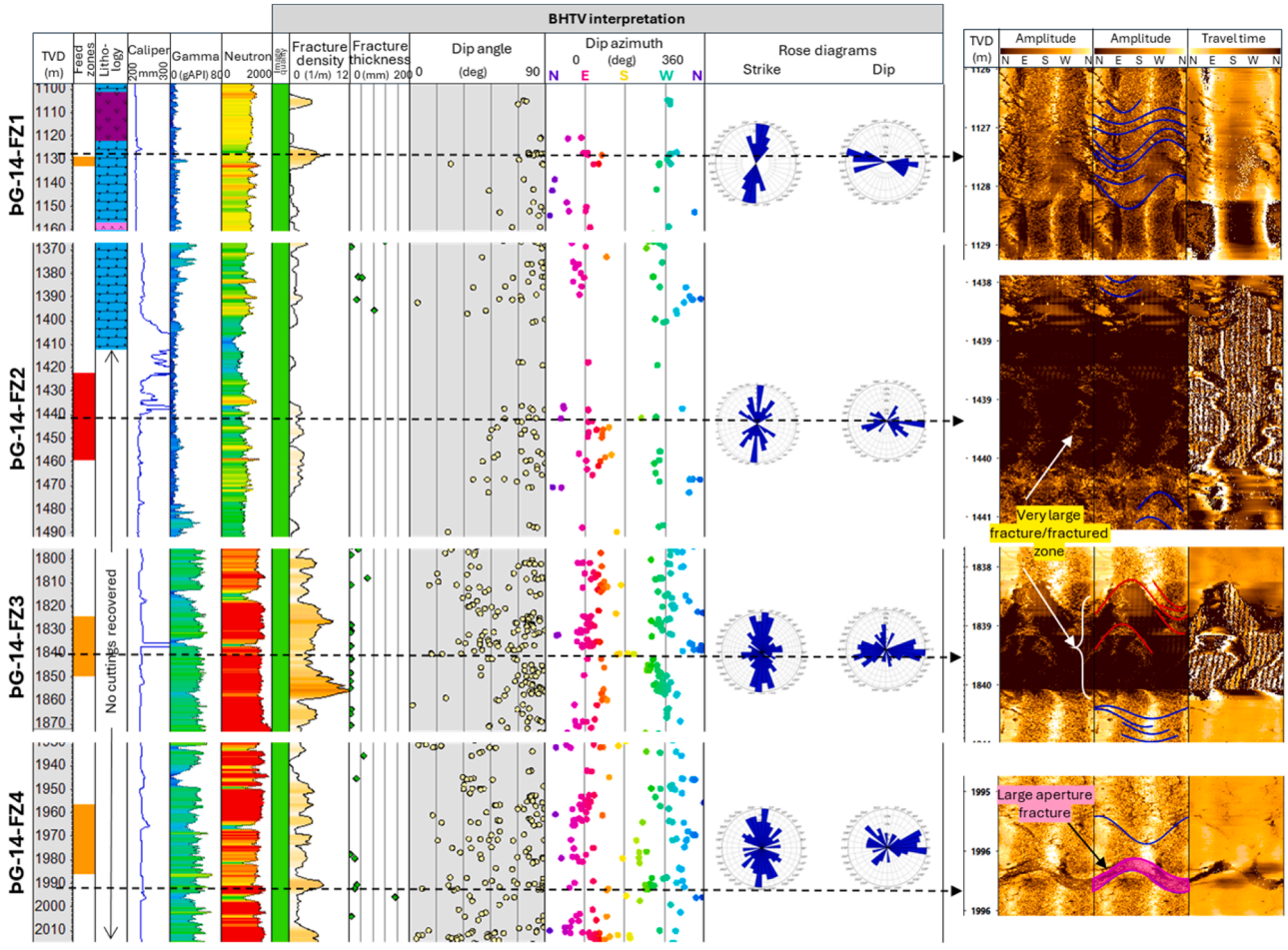

Fig. 9. Composite log in the major permeable zones of ÞG-14 showing the cuttings lithology, caliper log, gamma ray and neutron, along with the results of BHTV-fracture analysis. Image log quality, interpreted fracture density, thickness and orientations are represented. Rose diagrams of fractures in and around permeable feed zones are displayed in the last column. Structural features interpreted from televiewer images within these zones are shown on the right.

Individual fractures cannot be resolved, but the acoustic image response is indicative of a highly fractured or damage zone. A similar amplitude response is observed in the fracture interpreted at 1839 m, which is potentially linked to the feed zone around this depth (ÞG-14-FZ3). Moreover, the fracture density in this zone is also relatively higher (4–8 fracs/m) with thicknesses up to 8 mm. In contrast, the deepest feed zone (ÞG-14-FZ4) has moderate fracture densities between 2–5 fracs/m, but features a large 160 mm thick fracture below it at 1996 m depth. Fractures are generally steeply dipping with an overall N-S strike at each depth and a bimodal E and W dip distribution pattern. However, low to

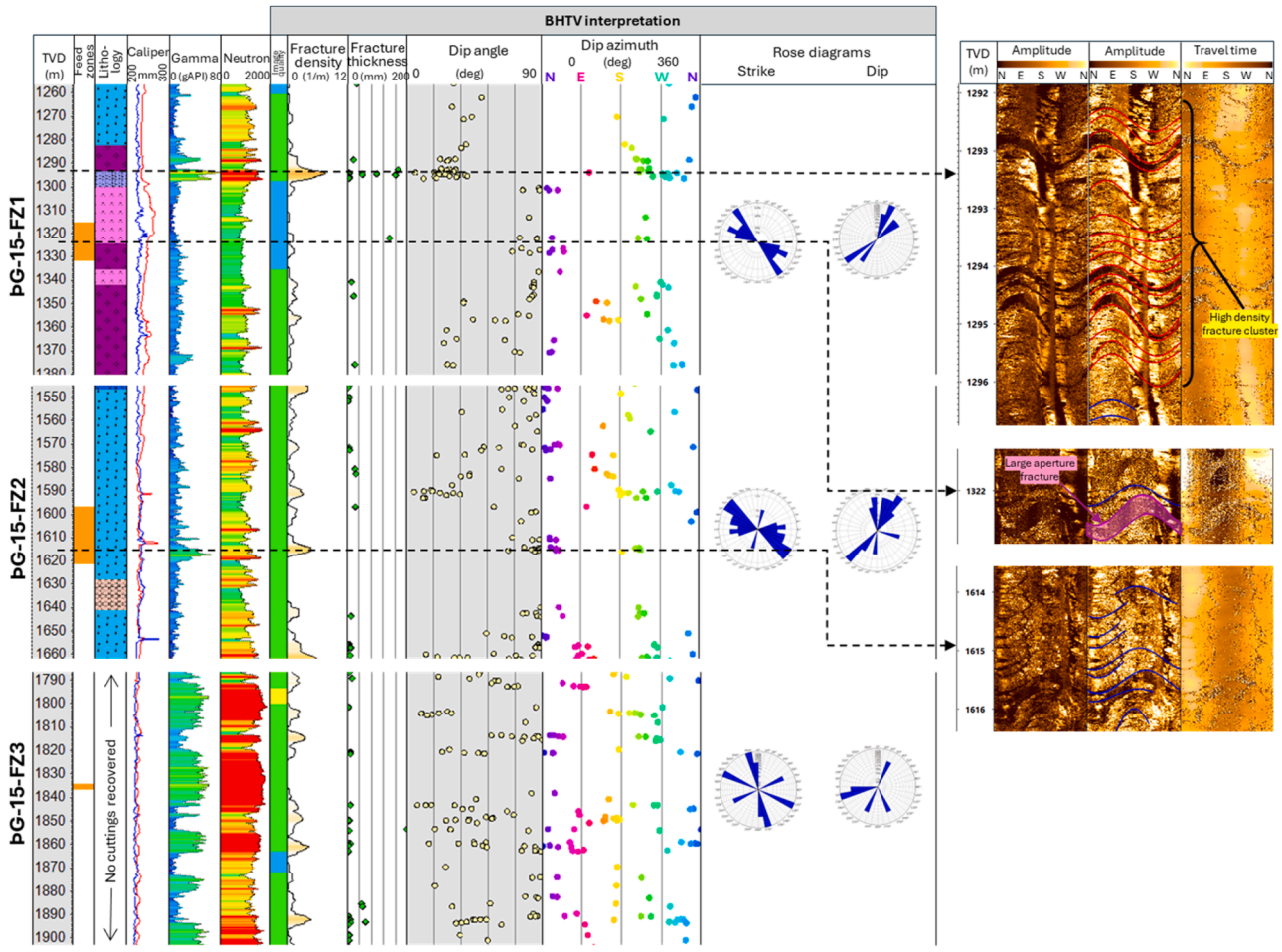

Fig. 10. Composite log in the major permeable zones of ÞG-15 showing the cuttings lithology, caliper log, gamma ray and neutron, along with the results of BHTV-fracture analysis. Image log quality, interpreted fracture density, thickness and orientations are represented. Rose diagrams of fractures in and around permeable feed zones are displayed in the last column. Structural features interpreted from televiewer images within these zones are shown on the right.

high dips angles are observed in the feed zones ÞG-14-FZ3 and ÞG-14-FZ4 within the acidic intrusive units.

Well ÞG-15

In ÞG-15, permeable zones are developed in hyaloclastite, basalt, and intrusive lithologies. A medium-sized feed zone (ÞG-15-FZ1) is identified in the hyaloclastite unit at 1315–1332 m (Fig. 10). Fracture strikes range from NNE-SSW to NW-SE around this depth. As shown in the BHTV images in Fig. 10, this feed zone possibly correlates with a high density fracture cluster at 1292–1296 m and the occurrence of a few large fractures with individual fracture thicknesses reaching up to 170 mm. ÞG-15-FZ2 (1597–1621 m) contains moderately dense fractures (0–4 frac/m), with NW–SE strikes, steep dips (>60°), and apertures up to 30 mm. A single very wide fracture (216 mm) occurs above the zone at 1590 m. Thus, ÞG-15 highlights the role of localized fracture corridors and large-aperture fractures in enhancing permeability. In contrast, ÞG-15-FZ3 within inter-acidic intrusion is poorly fractured with variable fracture strikes and <5 mm thicknesses.

Well ÞG-11

The first medium-sized feed zone is encountered in ÞG-11 at 922 m (Fig. 11), evidenced by the temperature and spinner logs. This feed zone consists of only a few fractures predominantly striking NE-SW. However, the gamma ray log suggests the presence of a small silicic intrusion at this depth. Similar feed zones associated with the occurrence of thin silicic intrusive veins are also observed in wells ÞG-12 and ÞG-17. ÞG-11-FZ2 (1380–1395 m) within hyaloclastite also shows very low fracture density and poor image quality. Fracture corridors are best developed at depth, within feed zones ÞG-11-FZ3 and ÞG-11-FZ4 hosting dense, multidirectional fracture networks (up to 9 frac/m) providing enhanced permeability. Fractures with thicknesses up to 25 mm and orientations ranging from NE-SW, NNE-SSW to N-S are observed in these zones. The feed zone at 1610–1625 m also possibly correlates with a formation contact at 1599 m as observed by the change in overall acoustic amplitude character at this depth shown in Fig. 11.

Well ÞG-12

The permeable feed zones in ÞG-12 are mainly hosted in hyaloclastite interbedded with basalt. The shallow feed zones (ÞG-12-FZ1 to ÞG-12-FZ3) are characterised by few fractures (<2 frac/m) with variable orientations, possibly due to the poor quality of borehole images within the hyaloclastite units (Fig. 12). The most significant fracture corridor is developed in ÞG-12-FZ4 (1785–1877 m), where fracture density increases up to 7 frac/m and fracture thickness reaches 40 mm. Fractures in this interval strike N–S, dip both east and west, and display a wide dip range (20–90°). The deeper basaltic zone (ÞG-12-FZ5) again shows poor structural development with very low fracture density.

Well ÞG-13

ÞG-13 exhibits a range of structural behaviour across lithologies and depth (Fig. 13). ÞG-13-FZ1 at 1182 m within hyaloclastite is poorly imaged and show little to no fractures at this depth. ÞG-13-FZ2 hosted in fine- to medium-grained basalt displays moderate fracture density (0–4 frac/m), with NE–SW striking, steeply dipping fractures that consistently dip NW. ÞG-13 exhibits structurally controlled permeability primarily in the deeper intrusive zone (ÞG-13-FZ3), where fracture corridors are best developed with systematic orientations (N–S to NE–SW strikes, W- to NW-dipping) and high variability in dip angles (30–90°).

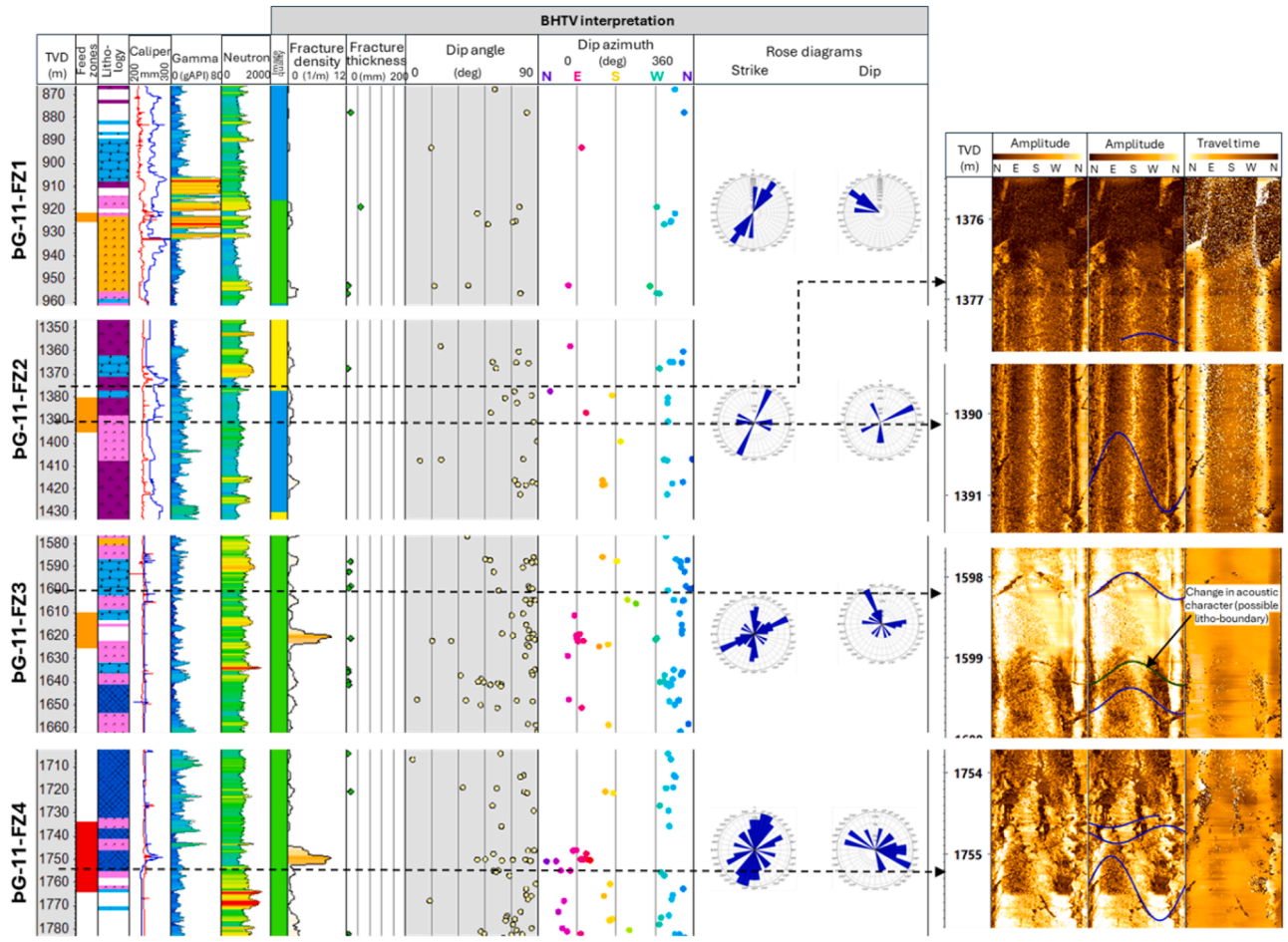

Fig. 11. Composite log in the major permeable zones of ÞG-11 showing the cuttings lithology, caliper log, gamma ray and neutron, along with the results of BHTV-fracture analysis. Image log quality, interpreted fracture density, thickness and orientations are represented. Rose diagrams of fractures in and around permeable feed zones are displayed in the last column. Structural features interpreted from televiewer images within these zones are shown on the right.

Well ÞG-17

The permeable feed zones in Well ÞG-17 occur across hyaloclastite and intrusive lithologies, with fracture development becoming more significant at depth (Fig. 14). In ÞG-17-FZ1 (1161 m), fractures are sparse and variably oriented, suggesting limited structural control. As depth increases into intrusive lithologies (FZ2–FZ4), fracture density rises significantly, dips remain moderate to steep and strikes ranging from N-S, NW-SE to E-W. The deepest zone, ÞG-17-FZ4, shows the best-developed fracture corridor with the highest density (up to 7 frac/m), thicker fractures, and consistent N–S striking, east-dipping geometries, forming a strong structural pathway for fluid movement.

5. Discussion: implications for permeability and fluid flow

Our structural analysis and comparison with feed zones highlights the highly heterogenous nature of permeable fractures in the reservoir. It is evident that assessing the contribution of fracture networks to permeability and preferential fluid flow pathways is not straightforward in the volcanic-hosted geothermal system in Þeistareykir. Earlier work in Icelandic geothermal systems has emphasized the role of rift-zone faults and fracture corridors within the active volcanic rift setting in focusing fluid flow (e.g., (Arnórsson, 1995; Liotta et al., 2021), and our observations confirm that these features also play a critical role in Þeistareykir. Several structural studies carried out at the surface in the Þeistareykir fissure swarm (e.g., Bonali et al., 2019; Pasquarè Mariotto et al., 2015; Tibaldi et al., 2020, 2016) document multiple fracture sets resulting from the combined influence of regional rifting, transfer-zone deformation associated with the Tjörnes Fracture Zone, and local structural inheritance. In particular, our borehole dataset of the dominant fracture orientations identified in the image logs (Fig. 6) mirror the surface-defined structural trends of the Þeistareykir fissure swarm—primarily the N–S, NNE–SSW and NE–SW striking sets, indicating that the mapped rift-parallel normal faults and open fissures exert a first-order control on the geometry of the deeper fracture network. This alignment suggests that many of the fractures encountered in the wells represent the down-dip continuation or secondary splays of the surface fault system, and that permeability is therefore strongly influenced by the structural architecture of the fissure swarm.

In addition to these broader patterns, our subsurface data also reveals a degree of finer-scale local variability that is not captured in surface structural maps. For example, the strong W- to NW-dipping fracture population in ÞG-13 and ÞG-11 contrasts with the more symmetric bimodal dip distributions in ÞG-12, ÞG-14 and ÞG-17 (Fig. 6 and 7). Such heterogeneity aligns with the interpretation of Tibaldi et al. (2020), who identified structural domains within the fissure swarm where fracture propagation is guided by deeper structures. Thus, the borehole data provide a deeper-scale continuation of the fracture architecture observed at the surface and support the interpretation that deformation in Þeistareykir is structurally partitioned. Furthermore, Bonali et al. (2019) showed that the geometry of the fracture system may deviate from the dominant regional trend due to dyke intrusions, local magmatic inflation or stress rotation. The broad dispersion of fracture orientations in ÞG-15 and rotated, shallower-dipping fractures in the deep intrusive units of ÞG-14 and ÞG-17 are consistent with such processes.

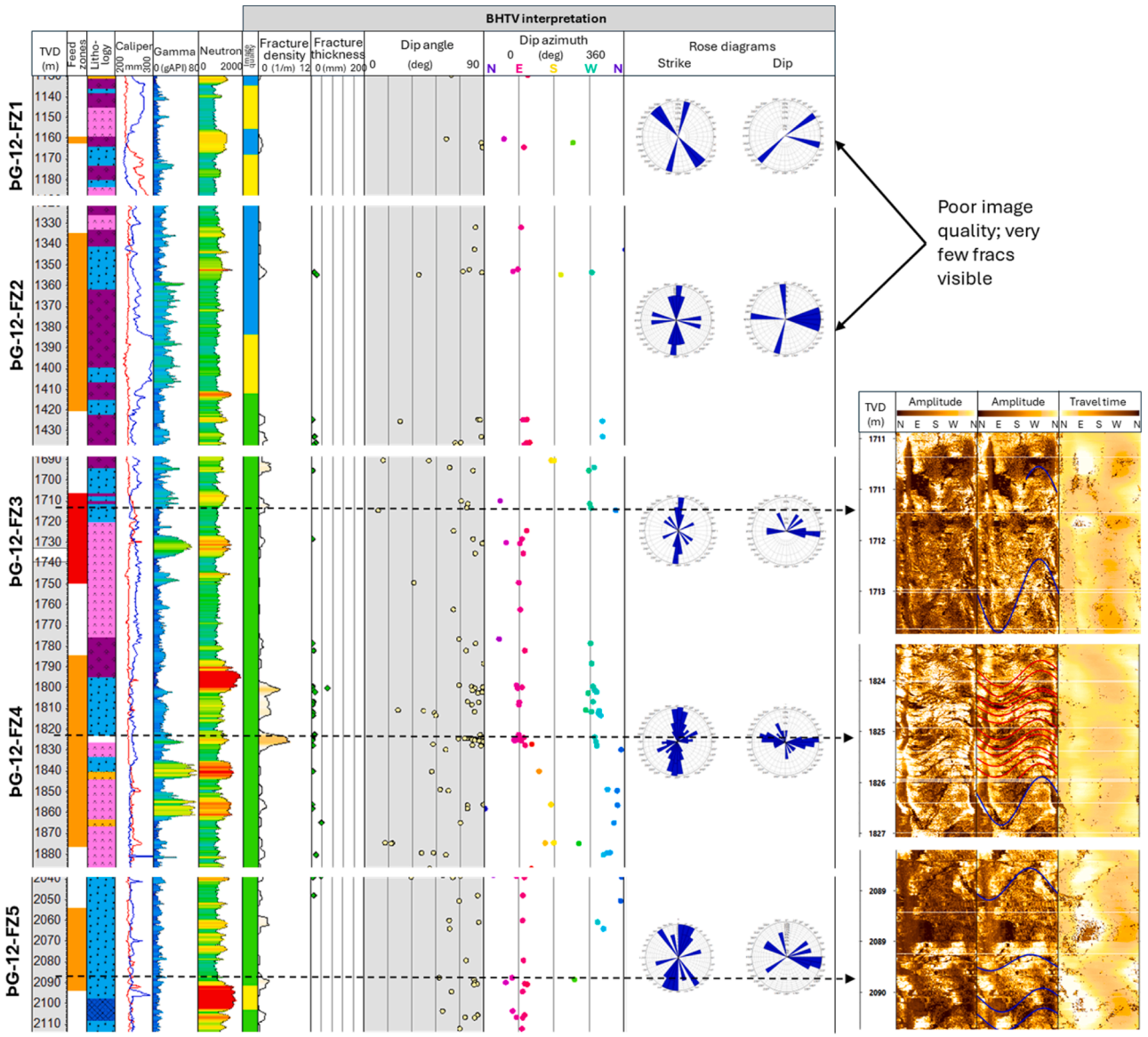

Fig. 12. Composite log in the major permeable zones of ÞG-12 showing the cuttings lithology, caliper log, gamma ray and neutron, along with the results of BHTV-fracture analysis. Image log quality, interpreted fracture density, thickness and orientations are represented. Rose diagrams of fractures in and around permeable feed zones are displayed in the last column. Structural features interpreted from televiewer images within these zones are shown on the right.

Most feed zones are characterized by diverse structural styles and variable degrees of fracture development. Permeability is strongly controlled by fractures but the relationship between permeable zones and fracture network geometry can vary significantly throughout the field. Moreover, interpretation of structural features from image logs is hindered by variable data quality, particularly in the shallower hyaloclastite units in wells ÞG-12, ÞG-13, and ÞG-11. Another limitation of BHTV analysis is that acoustic amplitude responses alone cannot distinguish between fully open and partially sealed fractures. Nevertheless, many feed zones show strong correlations with features visible in BHTV images. At times, high density fracture clusters dominate fluid flow (e.g. in ÞG-15) or in other cases, a single very large aperture fracture is found to be conductive (ÞG-14, ÞG-15). Permeability is also associated with an intensely fractured damage zone (e.g. in ÞG-14, Fig. 9) or a lithological boundary (e.g. Fig. 11) in some instances. Fractures within feed zones also do not necessarily exhibit a similar preferential orientation or a one-to-one correlation with any other fracture properties (Fig. 15). Fracture densities range from very sparse (0–2 fracs/m) to moderately developed intervals (up to 9 fracs/m). Feed zones also occur where few or no fractures are resolved (such as in wells ÞG-12 and ÞG-13), indicating that fracture density alone does not control permeability. Fracture apertures are generally narrow (5–20 mm), though occasional wider fractures (>50 mm) are present in ÞG-15 and ÞG-17. Dip angles range from shallow (20–30°) to near vertical (>70°), with dominant strikes including N–S, NW–SE, and NE–SW. Multiple dip directions are observed within most wells, often with both east- and west-dipping sets occurring together. This variability implies that permeability is supported by intersecting fracture networks rather than a single dominant orientation. Many wells, such as ÞG-12 and ÞG-15, display multiple fracture sets, while others (e.g., ÞG-13) are dominated by a single orientation. These combined observations demonstrate that feed zones in this field are structurally heterogeneous and permeability in the Þeistareykir geothermal reservoir is governed by the combination of a wide range of fracture system geometries (Fig. 15).

Another striking observation in this study is that less than ten percent of all interpreted fractures coincide with permeable feed zones, even though many fractures outside these zones also display similar orientations and characteristics as the permeable fractures. This strongly

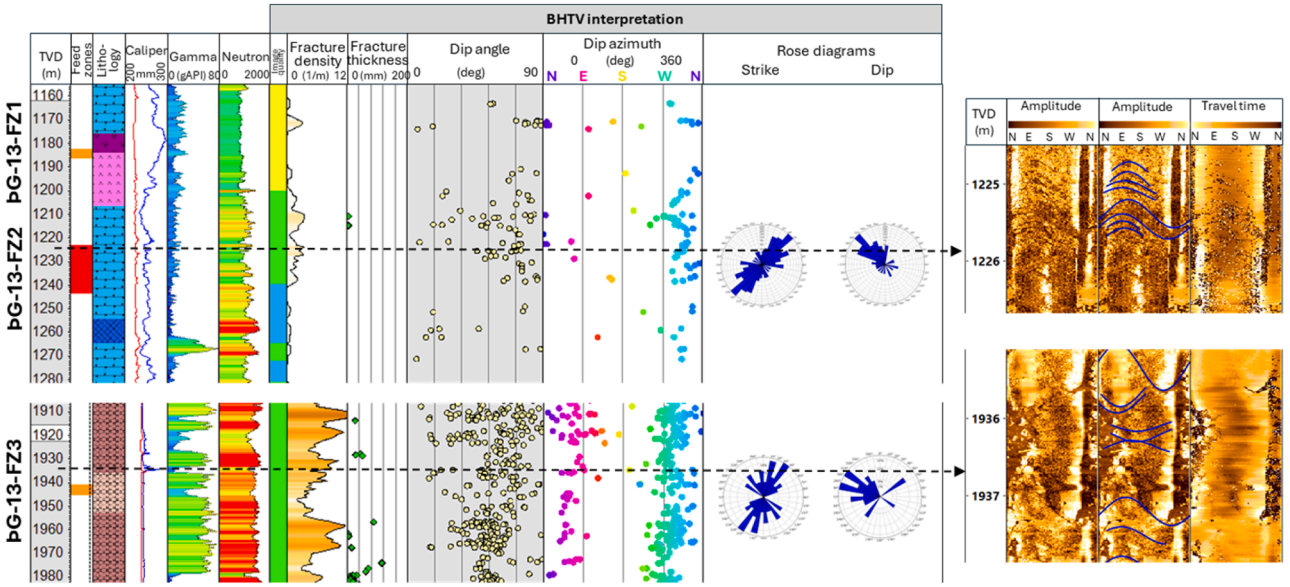

Fig. 13. Composite log in the major permeable zones of ÞG-13 showing the cuttings lithology, caliper log, gamma ray and neutron, along with the results of BHTV-fracture analysis. Image log quality, interpreted fracture density, thickness and orientations are represented. Rose diagrams of fractures in and around permeable feed zones are displayed in the last column. Structural features interpreted from televiewer images within these zones are shown on the right.

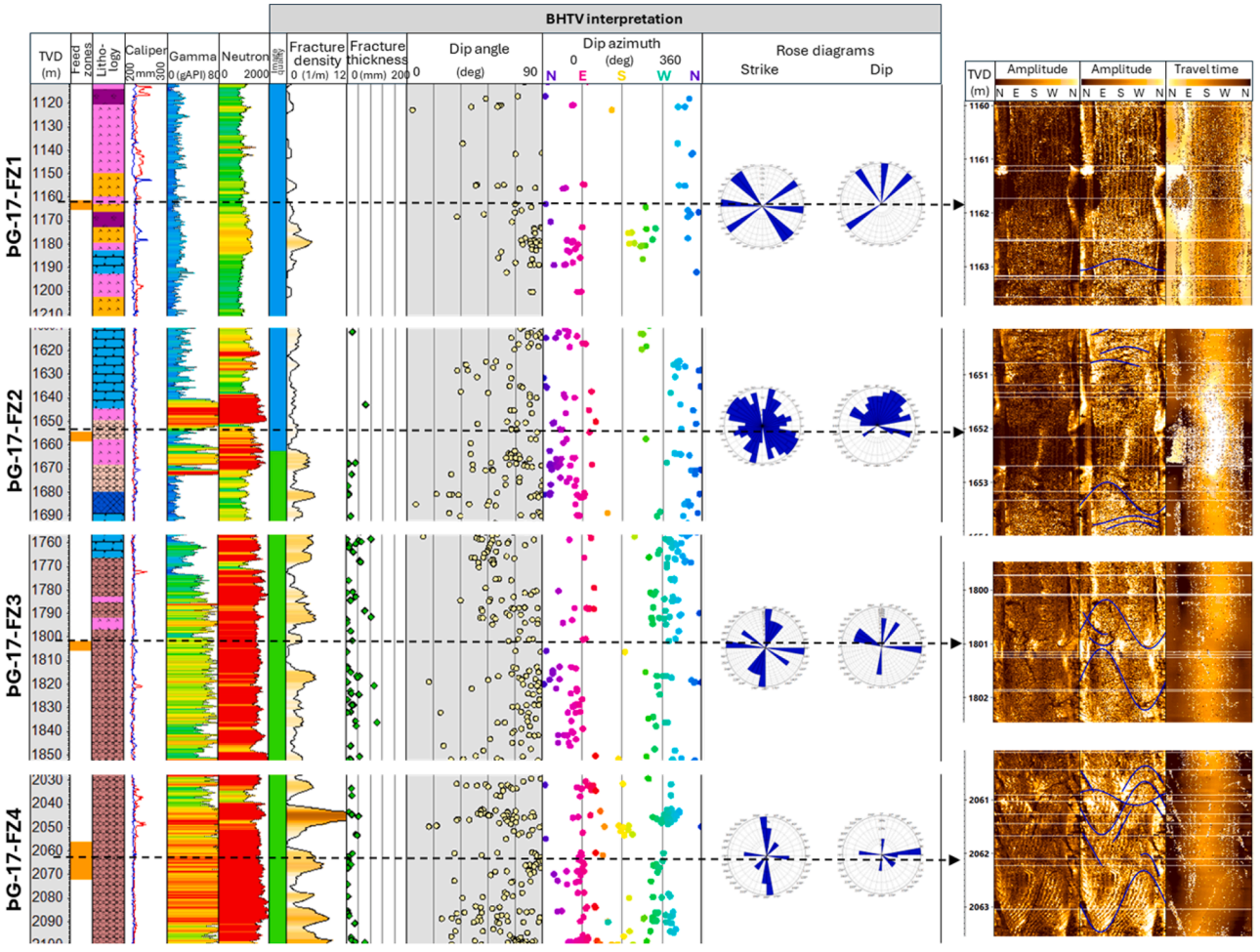

Fig. 14. Composite log in the major permeable zones of ÞG-17 showing the cuttings lithology, caliper log, gamma ray and neutron, along with the results of BHTV-fracture analysis. Image log quality, interpreted fracture density, thickness and orientations are represented. Rose diagrams of fractures in and around permeable feed zones are displayed in the last column. Structural features interpreted from televiewer images within these zones are shown on the right.

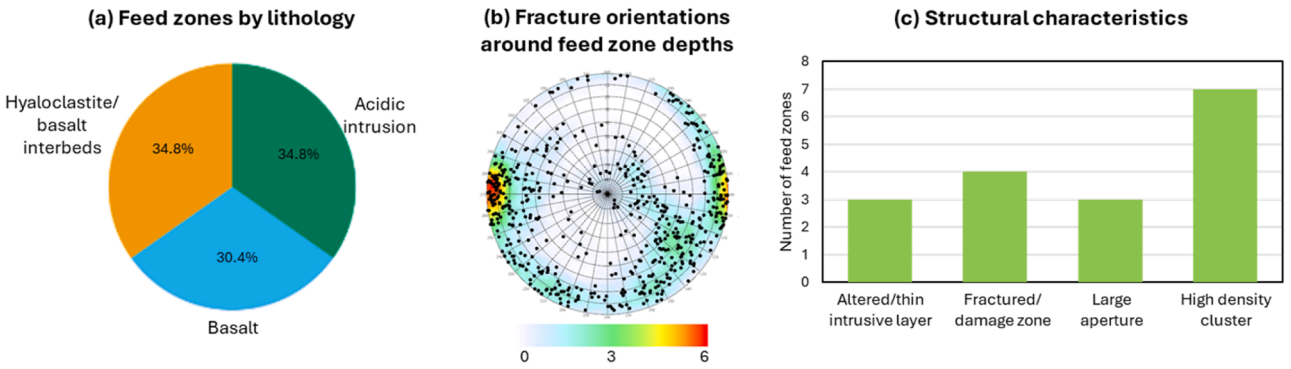

Fig. 15. Feed zone analysis results from all studied wells, (a) host lithology, (b) fracture orientations, and (c) observed structural characteristics around feed zone depths, revealing the heterogeneity in permeable fracture corridors within the Þeistareykir geothermal field.

indicates additional factors beyond simple fracture presence or abundance controlling fluid flow. Fracture-controlled permeability is highly selective and governed by the interplay of fracture orientations, host lithology, their structural position within the broader fault–fracture network, degree of connectivity, and the influence of mineralisation or hydrothermal alteration. Productive zones in borehole image logs are consistently linked to intersecting fracture corridors, large-aperture features, or intensely fractured damage zones, while adjacent intervals with similar fracture populations remain impermeable. Widespread mineral sealing of fractures (quartz/zeolites) observed in core analysis further reinforces this interpretation (Fig. 2). The self-sealing of fractures, especially via calcite precipitation, has been documented in fractured geothermal reservoirs such as Kawerau, where mineral infill reduces permeability over time (McNamara et al., 2016).

When viewed in a global context, our results align with studies of fracture-controlled geothermal systems elsewhere. In the Fallon area of Basin and Range Province of Nevada (USA), conjugate fracture sets identified using both FMS and BHTV image logs are likely to promote fluid flow in the geothermal system (Blake and Davatzes, 2012). This supports our own interpretation in Þeistareykir, where intersecting, multi-set fracture corridors appear to define key feed zones. Sone et al. (2023) further emphasise the strong well-to-well variability in conductive pathways at San Emidio geothermal field, with preferred flow mechanisms varying from large aperture fractures to more distributed fracture networks. Moreover, conductive fractures in their study do not always align with major surface faults, reinforcing our conclusion that permeability in Þeistareykir is governed by local fracture geometry and connectivity rather than regional structural trends alone. Studies from the Taupo Volcanic Zone of New Zealand demonstrate fault damage zones and intersections as primary fluid conduits (Rowland and Sibson, 2004), and permeability concentrated at intersecting structural trends, wide-aperture fractures and intervals of high fracture density (McNamara et al., 2019, 2015). Borehole image studies at Te Mihi (McNamara et al., 2019) and Rotokawa (McNamara et al., 2015) show the same spectrum of permeable expressions that we document at Þeistareykir: (1) high-intensity fracture corridors, (2) fractured damage zones that provide distributed connectivity, (2) discrete large-aperture fractures that can dominate local flow. Our observations at Þeistareykir therefore support a more general model of geothermal permeability in volcanic rift zones. There are important contrasts, however, that refine how the global analogues should be applied. Compared with the TVZ and Nevada Basin and Range, where good image log to core ties sometimes allow clearer discrimination between open versus sealed fractures (Davatzes and Hickman, 2010; Milloy et al., 2015), the lack of core from deeper reservoir unit in Þeistareykir, widespread alteration and frequent poor image quality in hyaloclastite make that discrimination harder and increase uncertainty in identifying flow-supporting features.

Beyond these comparisons, the Þeistareykir results also highlight several practical implications for geothermal resource development. The presence of intersecting fracture corridors within major feed zones suggests that well trajectories that maximise the intersection of multiple fracture sets—particularly both rift-parallel and oblique sets—may yield higher permeability. Lithological boundaries and small intrusive contacts also appear to play an important role, indicating that these interfaces may serve as favourable drilling targets. The results also highlight the need for discrete and spatially variable fracture inputs in reservoir modelling rather than uniform permeability fields. Future work will involve (1) exploring the impact of the tectonic stress environment on subsurface fractures, (2) incorporating the observed fracture variability from this study into building discrete fracture network (DFN) models, and (3) integrating with the regional fault models, to improve predictions of bulk permeability distribution in the reservoir and lead to more realistic models of fluid flow.

6. Conclusion

In the geothermal system of Þeistareykir, we present a detailed structural characterization of fracture networks and permeable flow zones in the reservoir based on core observations, borehole image log analysis, drilling and well logging data from the Þeistareykir geothermal field. Fractures exhibit a heterogeneous distribution and orientation pattern within the field. The observed spatial variability in the fracture strikes ranges from NNW-SSE, N-S, NNE-SSW to NE-SW, with bimodal dip distribution and low to high dip angles (0–90°). The N-S and NE-SW trending fractures are better defined, with a higher concentration of data and mirroring the regional structural trend in the area, while the other fracture orientations display a more dispersed pattern, possibly related to secondary faults. The overall fracture thicknesses calculated from image analysis are relatively uniform in the order of 1–50 mm throughout the field. While basaltic and intrusive lithologies tend to host more fractures than hyaloclastite units, permeable feed zones are not uniformly associated with high fracture densities. Instead, permeability is often localized within diverse geometry and structural styles including high density fracture clusters and damage zones, very large aperture fractures, litho-boundary and small silicic intrusions. Fracture strikes and dips also vary widely, implying that fluid flow is accommodated by multiple intersecting fracture sets rather than a single dominant orientation. These results reveal the highly variable nature of the structural controls on reservoir permeability and fluid flow channels in the Þeistareykir geothermal system. Beyond advancing the understanding of Þeistareykir, this study provides a framework for fracture network characterization in other structurally complex geothermal systems worldwide, ultimately aiding in resource assessment and reservoir management.

CRediT authorship contribution statement

Aastha: Writing – original draft, Visualization, Methodology, Investigation, Conceptualization. **Emma Bramham:** Writing – review & editing, Supervision, Conceptualization. **Andy Nowacki:** Writing – review & editing, Supervision, Conceptualization. **Nick Shaw:** Writing – review & editing, Supervision, Conceptualization. **Anette Mortensen:** Writing – review & editing, Supervision, Conceptualization. **David Healy:** Writing – review & editing, Supervision.

Declaration of competing interest

The authors declare that they have no known competing financial interests or personal relationships that could have appeared to influence the work reported in this paper.

Acknowledgement

This work is part of the PhD project of the lead author which is supported by the Natural Environment Research Council [grant number NE/S007458/1]. AN is supported by NERC (NE/T012684/1) and Geosolutions Leeds.

Supplementary materials

Supplementary material associated with this article can be found, in the online version, at doi:10.1016/j.geothermics.2026.103596.

Data availability

All the data used in this research belongs to Landsvirkjun and can be made available upon request to Landsvirkjun co-author Anette Mortensen.

References

Ármannsson, H., 2016. The fluid geochemistry of Icelandic high temperature geothermal areas. Appl. Geochem. 66, 14–64. https://doi.org/10.1016/j.apgeochem.2015.10.008.

Arnórsson, S., 1995. Geothermal systems in Iceland: structure and conceptual models—i. High-temperature areas. Geothermics 24, 561–602. https://doi.org/10.1016/0375-6505(95)00025-9.

Ásgeirsdóttir, R.S., Sigurgeirsson, M.Á., Guðjónsdóttir, S.R., Tryggvason, H.H., Egilson, Þ., Guðmundsdóttir, V., Pétursson, F., Vilhjálmsson, S., Ingólfsson, H., Stefánsson, H.Ö., 2017a. Þeistareykir – well ÞG-17. phase 3: drilling for 7" perforated liner down to 2500 m (No. LV-2017–092). a. Landsvirkjun.

Ásgeirsdóttir, R.S., Sigurgeirsson, M.Á., Guðmundsdóttir, V., Tryggvason, H., Egilson, Þ., Guðjónsdóttir, S.R., Pétursson, F., Ingólfsson, H., Sveinbjörnsson, S., Árnadóttir, S., Stefánsson, H.Ö., Kristinsson, B., Sveinbjörnsson, B.M., 2017b. Þeistareykir - Well ÞG-13 Phase 3: Drilling for a 7" Perforated Liner Down to 2505 m Depth (No. LV-2017–020). b. Landsvirkjun.

Ásgeirsdóttir, R.St., Poux, B., Guðjónsdóttir, S.R., Sigurgeirsson, M.Á., Tryggvason, H., Egilson, Þ., Stefánsson, H.Ö., Ingimarsson, H., Árnadóttir, S., Sveinbjörnsson, S., 2016. Þeistareykir - Well ÞG-12 phase 3: drilling the production part from 806 m to 2710 m depth (No. LV-2016–121). Landsvirkjun.

Bense, V.F., Gleeson, T., Loveless, S.E., Bour, O., Scibek, J., 2013. Fault zone hydrogeology. Earth-Sci. Rev. 127, 171–192. https://doi.org/10.1016/j.earscirev.2013.09.008.

Blake, K., Davatzes, N., 2012. Borehole image log and statistical analysis of FOH-3D, fallon naval air station, NV. 37th Workshop On Geothermal Reservoir Engineering. Stanford University, Stanford, California.

Bonali, F.L., Tibaldi, A., Mariotto, F.P., Saviano, D., Meloni, A., Sajovitz, P., 2019. Geometry, oblique kinematics and extensional strain variation along a diverging plate boundary: the example of the northern Theistareykir Fissure Swarm. NE Icel. Tectonophys. 756, 57–72. https://doi.org/10.1016/j.tecto.2019.02.018.

Brandão, A.G., Wennberg, O.P., Borghi, L., Oliveira, J.P., Carneiro, V., 2024. Fracture analysis in borehole images from bm-c-33 area, outer campos basin, brazil. PG 30, petgeo2023-134. https://doi.org/10.1144/petgeo2023-134.

Brogi, A., 2008. Fault zone architecture and permeability features in siliceous sedimentary rocks: insights from the Rapolano geothermal area (Northern Apennines, Italy). J. Struct. Geol. 30, 237–256. https://doi.org/10.1016/j.jsg.2007.10.004.

Caine, J.S., Evans, J.P., Forster, C.B., 1996. Fault zone architecture and permeability structure. Geology 24, 1025–1028. https://doi.org/10.1130/0091-7613(1996)024<1025:FZAAPS>2.3.CO;2.

Camps, P., Singer, B.S., Carvallo, C., Goguitchaichvili, A., Fanjat, G., Allen, B., 2011. The Kamikatsura event and the matuyama–brunhes reversal recorded in lavas from Tjörnes peninsula, northern iceland. Earth Planet. Sci. Lett 310, 33–44. https://doi.org/10.1016/j.epsl.2011.07.026.

Chen, B.-C., Perdana, T., Kuo, L.-W., 2021. Fluid flow and fault-related subsurface fractures in slate and metasandstone formations: a case study of the Jentse Geothermal Area, Taiwan. Geothermics 89, 101986. https://doi.org/10.1016/j.geothermics.2020.101986.

Davatzes, N., Hickman, S., 2010. Stress, Fracture and Fluid Flow Analysis Using Acoustic and Electrical Image Logs in Fractured Granites of the Coso Geothermal Field. AAPG Memoir, Nevada, pp. 259–293. https://doi.org/10.1306/13181288M923134.

Dezayes, C., Valley, B., Maqua, E., Syren, G., Genter, A., 2005. Natural fracture system of the Soultz granite based on UBI data in the GPK3 and GPK4 wells. In: Presented at the EHDRA scientific conference.

Einarsson, P., 2008. Plate boundaries, rifts and transforms in Iceland. Jök 58, 35–58. https://doi.org/10.33799/jokull2008.58.035.

Faulds, J., Hinz, N., 2015. Favorable Tectonic and Structural Settings of Geothermal Systems in the Great Basin Region, Western USA: proxies for Discovering Blind Geothermal Systems. In: Proceedings World Geothermal Congress 2015. Melbourne, Australia.

Gíslason, G., Johnsen, G.V., Ármannsson, H., Torfason, H., Árnason, K., 1984. Theistareykir. Surface exploration of the High-Temperature Geothermal area. Orkustofnun, Reykjavík, Rep. No. OS 84089/JHD16 134.

Guðjónsdóttir, S.R., Guðmundsdóttir, V., Sigurgeirsson, M., Ásgeirsdóttir, R.S., Tryggvason, H.H., Stefánsson, H.Ö., Ingólfsson, H., Pétursson, F., Gunnarsson, B.S., Egilson, Þ., 2017. Þeistareykir – Well ÞG-14. Phase 3: drilling for a 7" perforated liner down to 2500 m (technical report no. ÍSOR-2017/023). Iceland Geosurvey.

Guðmundsdóttir, V., Þorgilsson, G., Egilson, Þ., 2018. Spinner log processing and permeability distribution in the þeistareykir geothermal reservoir (technical report No. ÍSOR-2018/084). Iceland GeoSurvey.

Hjartardóttir, Á., 2013. Fissure swarms of the northern volcanic rift zone, Iceland (PhD Thesis). University of Iceland.

Hjartardóttir, Á.R., Einarsson, P., Magnúsdóttir, S., Björnsdóttir, Þ., Brandsdóttir, B., 2016. Fracture systems of the northern volcanic rift zone, iceland: an onshore part of the mid-atlantic plate boundary. Geol. Soc. 420, 297–314. https://doi.org/10.1144/SP420.1. London, Special Publications.

Hosseini, E., Ghojogh, J.N., Habibnia, B., 2015. Study of faults in Asmari formation by FMI image log, case study: lali oilfield. Am. J. Oil Chem. Technol.: Vol. 3.

Borehole Images Hurley, N., 2004. In: Asquith, G., Krygowski, D., Henderson, S., Hurley, N. (Eds.), Basic Well Log Analysis. American Association of Petroleum Geologists, p. 0. https://doi.org/10.1306/Mth16823C9.

Jóhannsson, J.Ú., 2011. Þeistareykir high-temperature geothermal field, north-east iceland : estimation of reservoir conditions and evaluation of pressure interference Between Wells (MSc Thesis).

Kajugus, S.I., 2012. Updated reservoir analysis of the theistareykir high-temperature geothermal field, N-Iceland. UNU-GTP, Reykjavik, Iceland.

Karlsdóttir, R., Vilhjálmsson, A., Árnason, K., Beyene, A., 2012. Þeistareykir geothermal area, northern Iceland 3D inversion of mt and tem data, p. 173. Reykjavík (No. ÍSOR-2012/046).

Khodayar, M., Björnsson, S., Kristinsson, S.G., Karlsdóttir, R., Ólafsson, M., Víkingsson, S., 2018. Tectonic control of the theistareykir geothermal field by rift and transform zones in north iceland: a multidisciplinary approach. OJG 08, 543–584. https://doi.org/10.4236/ojg.2018.86033.

Kraal, K.O., Ayling, B.F., Blake, K., Hackett, L., Perdana, T.S.P., Stacey, R., 2021. Linkages between hydrothermal alteration, natural fractures, and permeability: integration of borehole data for reservoir characterization at the Fallon FORGE EGS site, Nevada, USA. Geothermics 89, 101946. https://doi.org/10.1016/j.geothermics.2020.101946.

Kulander, B.R., Dean, S.L., Ward, B.J., Jr, 1990. Fractured core analysis: interpretation, logging, and use of natural and induced fractures in core. American Association of Petroleum Geologists. https://doi.org/10.1306/Mth8516.

Lacasse, C., Guðmundsson, G., Þrastarson, R.H., Elefsen, S.Ó., 2007. Boreholes ÞR-7, GR-3 in northeast iceland - geology and temperature loggings (no. VH 2007-125). VGK-Hönnun.

Lai, J., Wang, G., Wang, S., Cao, J., Li, M., Pang, X., Han, C., Fan, X., Yang, L., He, Z., Qin, Z., 2018. A review on the applications of image logs in structural analysis and sedimentary characterization. Mar. Pet. Geol. 95, 139–166. https://doi.org/10.1016/j.marpetgeo.2018.04.020.

Liotta, D., Brogi, A., Árnadóttir, S., Ágústsson, K., Thorsteinsdóttir, U., 2021. Field evidence of the interplay between rift and transform structures in the Krafla geothermal area, N-Iceland. Geothermics 91, 102039. https://doi.org/10.1016/j.geothermics.2020.102039.

Magnúsdóttir, S., Brandsdóttir, B., 2011. Tectonics of the Þeistareykir fissure swarm. Jökull 61, 65–79. https://doi.org/10.33799/jokull2011.61.065.

Massiot, C., McNamara, D.D., Lewis, B., 2015. Processing and analysis of high temperature geothermal acoustic borehole image logs in the Taupo Volcanic Zone, New Zealand. Geothermics 53, 190–201. https://doi.org/10.1016/j.geothermics.2014.05.010.

McNamara, D.D., Lister, A., Prior, D.J., 2016. Calcite sealing in a fractured geothermal reservoir: insights from combined EBSD and chemistry mapping. J. Volcanol. Geotherm. Res. 323, 38–52. https://doi.org/10.1016/j.jvolgeores.2016.04.042.

McNamara, D.D., Massiot, C., Lewis, B., Wallis, I.C., 2015. Heterogeneity of structure and stress in the Rotokawa Geothermal Field, New Zealand. J. Geophys. Res.: Solid Earth 120, 1243–1262. https://doi.org/10.1002/2014JB011480.

McNamara, D.D., Milicich, S.D., Massiot, C., Villamor, P., McLean, K., Sépulveda, F., Ries, W.F., 2019. Tectonic Controls on Taupo Volcanic Zone Geothermal Expression:

insights From Te Mihi, Wairakei Geothermal Field. Tectonics 38, 3011–3033. https://doi.org/10.1029/2018TC005296.
Milloy, S.F., McLean, K., McNamara, D.D., 2015. Comparing borehole televiewer logs with continuous core: an example from New Zealand. In: Proceedings World Geothermal Congress 2015. Melbourne, Australia.
Mutonga, M.W., Fujimitsu, Y., 2024. Identification of natural subsurface structures using borehole images, temperature logs and pertinent data: a case study of the Menengai geothermal field. Kenya. Geoenergy Sci. Eng. 237, 212797. https://doi.org/10.1016/j.geoen.2024.212797.
Narr, W., Schechter, D.S., Thompson, L.B., 2006. Naturally fractured reservoir characterization. Soc. Pet. Eng. https://doi.org/10.2118/9781613999615.
Óskarsson, F., 2016. Exploration and development of a conceptual model for the theistareykir geothermal field, NE-Iceland. SDG Short Course I on Exploration and Development of Geothermal Resources. UNU-GTP, Kenya.
Pasquarè Mariotto, F., Bonali, F.L., Tibaldi, A., Rust, D., Oppizzi, P., Cavallo, A., 2015. Holocene displacement field at an emerged oceanic transform-ridge junction: the Husavik-Flatey Fault – Gudfinnugja Fault system, North Iceland. J Struct Geol 75, 118–134. https://doi.org/10.1016/j.jsg.2015.03.011.
Pedersen, R., Sigmundsson, F., Masterlark, T., 2009. Rheologic controls on inter-rifting deformation of the Northern Volcanic Zone. Icel. Earth Planet. Sci. Lett. 281, 14–26. https://doi.org/10.1016/j.epsl.2009.02.003.
Pérez-Flores, P., Veloso, E., Cembrano, J., Sánchez-Alfaro, P., Lizama, M., Arancibia, G., 2017. Fracture network, fluid pathways and paleostress at the Tolhuaca geothermal field. J. Struct. Geol. 96, 134–148. https://doi.org/10.1016/j.jsg.2017.01.009.
Poppelreiter, M., Garcia-Carballido, C., Kraaijveld, M., 2010. Borehole Image Log Technology: application Across the Exploration and Production Life Cycle 1–13. https://doi.org/10.1306/13181274M923406.
Poux, B., Ásgeirsdóttir, R., Guðjónsdóttir, Sylvía Rakel, Sigurgeirsson, Magnús Á., Gautason, B., Egilson, Þ., Sveinbjörnsson, S., Pétursson, F., Ingimarsson, H., Millachine, M.T., Stefánsson, H.Ö., Thordarson, S., 2016. Þeistareykir - Well ÞG-11 Phase 3: drilling for the production section for a 7" liner from 802 m to 2224 m depth (No. LV-2016–107). Landsvirkjun.
Rowland, J.V., Sibson, R.H., 2004. Structural controls on hydrothermal flow in a segmented rift system, Taupo Volcanic Zone, New Zealand. Geofluids 4, 259–283. https://doi.org/10.1111/j.1468-8123.2004.00091.x.
Saby, M., Pinti, D.L., Van Hinsberg, V., Gautason, B., Sigurðardóttir, Á., Castro, C., Hall, C., Óskarsson, F., Rocher, O., Hélie, J.-F., Méjean, P., 2020. Sources and transport of fluid and heat at the newly-developed Theistareykir Geothermal Field, Iceland. J. Volcanol. Geotherm. Res. 405, 107062. https://doi.org/10.1016/j.jvolgeores.2020.107062.
Sæmundsson, K., 2007. Geology of þeistareykir (in Icelandic). (Iceland Geosurvey, short report no. ÍSOR-07270).
Sæmundsson, K., 1974. Evolution of the axial rifting zone in northern Iceland and the Tjörnes fracture zone. GSA Bull. 85, 495–504. https://doi.org/10.1130/0016-7606(1974)85<495:EOTARZ>2.0.CO;2.
Sæmundsson, K., Hjartarson, Á., Kaldal, I., Sigurgeirsson, M.Á., Kristinsson, S.G., Víkingsson, S., 2012. Geological map of northern volcanic zone, Iceland. northern part.
Sibson, R.H., 1996. Structural permeability of fluid-driven fault-fracture meshes. J. Struct. Geol. 18, 1031–1042. https://doi.org/10.1016/0191-8141(96)00032-6.
Sigurgeirsson, M.Á., Guðjónsdóttir, S.R., Ásgeirsdóttir, R.S., Tryggvason, H.H., Egilson, Þ., Guðmundsdóttir, V., Gunnarsson, B.S., Vilhjálmsson, S., Ingimarsson, H., Pétursson, F., Ingólfsson, H., 2017. Þeistareykir - Well ÞG-15 phase 3: drilling for a 7" perforated liner down to 2260 m (No. LV-2017–047). Landsvirkjun.
Sone, H., Mudatsir, O., Jin, Z., Folsom, M., Ramirez, G., Feigl, K.L., 2023. WHOLESCALE - characterization of conductive fractured zones based on borehole data at san emidio geothermal field, Nevada. 48th Workshop on geothermal reservoir engineering. Stanford University, Stanford, California.
Steingrímsson, B., 2011. Geothermal Well Logging: geological Wireline Logs and Fracture Imaging. Short course on geothermal drilling, resource development and power plants. UNU-GTP.
Sveinbjornsdottir, Á.E., Ármannsson, H., Ólafsson, M., Óskarsson, F., Markússon, S., Magnusdottir, S., 2013. The theistareykir geothermal field, ne iceland. isotopic characteristics and origin of circulating fluids. procedia earth and planetary science, proceedings of the fourteenth international symposium on water-rock interaction, WRI 14 7, 822–825. https://doi.org/10.1016/j.proeps.2013.03.171.
Tavakoli, V., 2018. Geological core analysis, springerbriefs in petroleum geoscience & engineering. Springer International Publishing, Cham. https://doi.org/10.1007/978-3-319-78027-6.
Terzaghi, R.D., 1965. Sources of Error in Joint Surveys. Geotechnique 15, 287–304. https://doi.org/10.1680/geot.1965.15.3.287.
Tibaldi, A., Bonali, F.L., Einarsson, P., Hjartardóttir, Á.R., Pasquarè Mariotto, F.A., 2016. Partitioning of Holocene kinematics and interaction between the theistareykir fissure swarm and the husavik-flatey fault, north Iceland. J. Struct. Geol. 83, 134–155. https://doi.org/10.1016/j.jsg.2016.01.003.
Tibaldi, A., Bonali, F.L., Pasquaré Mariotto, F., Corti, N., Russo, E., Einarsson, P., Hjartardóttir, Á.R., 2020. Rifting kinematics produced by magmatic and tectonic stresses in the north Volcanic zone of Iceland. Front. Earth Sci. 8. https://doi.org/10.3389/feart.2020.00174.
Wennberg, O.P., De Oliveira Ramalho, F., Virgolino Mafia, M., Lapponi, F., Chandler, A. S., Gomis Cartesio, L.E., Hunt, D.W., 2023. The characteristics of natural open fractures in acoustic borehole image logs from the pre-salt Barra Velha formation, Santos basin, Brazil. J. Struct. Geol. 167, 104794. https://doi.org/10.1016/j.jsg.2023.104794.
Zahmatkesh, I., Aghli, G., Mohamadian, R., 2016. Systematic fractures analysis using image logs and complementary methods in the Marun Oilfield, SW Iran. Geopersia 5, 139–150.
Zemanek, J.O.E., Glenn, E.E., Norton, L.J., Caldwell, R.L., 1970. Formation evaluation by inspection with the borehole televiewer. Geophysics 35, 254–269.